



Analysis, optimization and evaluation of a pipe inspection robot

Harm de Boer

MSc report

Supervisors:

prof.dr.ir. S. Stramigioli

ir. E..C. Dertien

prof.dr.ir. P.P.L. Regtien

August 2008

Report nr. 028CE2008

Control Engineering

EE-Math-CS

University of Twente

P.O.Box 217

7500 AE Enschede

The Netherlands

Summary

Gas main inspection in urban areas is very time consuming and expensive. This is why a first robot prototype has been built which can inspect autonomously the pipe network from inside the pipe. However the currently available prototype does not satisfy all the requirements that have to be fulfilled for the first prototype. This master's thesis focuses on a small subset of those requirements e.g. the manoeuvring requirements. The currently constructed prototype is analyzed, optimised and evaluated in relation to the manoeuvring requirements.

First the shortcomings of the existing prototype in relation to the required manoeuvres, were determined. Moving up a slope of 30° and through a T-joint is problematic. Also the average speed requirement of 80 mm/s cannot be met. The shortcomings of the existing prototype in relation to these manoeuvres, are analysed for the different prototype modules.

The mechanical construction of the bending module has been optimized to reduce friction, which improved the clamping torque. The maximum necessary clamping torque could not be theoretically determined, because the friction coefficient between the wheel and pipe wall is too high to measure. This high friction coefficient is caused by the deformation of the wheels. However, it can be concluded that the necessary clamp torque that the bending modules can deliver, is sufficient for the different manoeuvres. The overall efficiency of the bending module is low, which is caused by the low clamping speed of approximately (14 mm/s). Using the motor current as clamp torque feedback seems to be a better solution than using the torsion spring elongation. An advantage of using the motor current for control, is that excessive stress on the motors is limited. Also the zero reference is much more accurate and the deviation of the torque as function of the motor current is low. A disadvantage is that only one motor at a time can be used.

From the driving module analysis it can be concluded that the driving motors cannot provide the maximum necessary torque at the nominal motor current. This maximum necessary torque is approximately 131 mNm, while the driving torque at the nominal motor current is approximately 120 mNm. The efficiencies of the driving module are low. These low efficiencies are caused by friction between the gears. The driving speed is approximately 70 mm/s and less above driving torques of 120 mNm. Because the bending speed is also low, the speed requirement of 80 mm/s cannot be met. For driving autonomously, it is recommended to use position/speed control in combination with the motor current control. This prevents excessive stress on the motor.

From the rotation module analysis it can be concluded that the rotation motor can deliver the necessary theoretical torque. During the analysis of the limitations of the current prototype, it has also been determined that the rotation module can practically deliver the necessary rotation torque in the worst case situation. Therefore, the rotation module does not have to be optimized.

From the performance evaluation of the total pipe inspection robot with respect to all the required manoeuvres, it can be concluded that the bending module optimizations increased the manoeuvrability of the prototype. Almost all manoeuvre requirements can be met, except for driving sideways up a slope of 30° . A reason for not meeting this manoeuvre is that the wheels deform slightly when driving sideways, giving a reduction of the possible torque of 40 mNm. Also the speed requirement cannot be met by the optimized prototype. To increase the driving torque the current gearbox can be replaced by the Faulhaber 15A, which has a higher reduction. However the driving speed will then decrease because of these extra reductions. Instead of increasing the driving torque, it would be better to reduce the friction caused by the clamping torque. Experimenting with different kinds of rubber and shape might create a more suitable trade-off between the traction and driving torque.

Samenvatting

De huidige methoden van gasleidinginspectie kosten veel tijd en geld. Om deze redenen is er een eerste prototype gebouwd van een robot die autonoom van binnenuit het gasleiding netwerk kan inspecteren. Het huidige prototype kan alleen nog niet voldoen aan alle gestelde eisen. Dit onderzoek richt zich op het behalen van een gedeelte van die eisen, namelijk de manoeuvreer eisen. Het huidige prototype is, met betrekking tot het behalen van deze eisen, geanalyseerd, geoptimaliseerd en geëvalueerd.

Eerst zijn de tekortkomingen van het huidige prototype met betrekking tot de gestelde manoeuvreer eisen geanalyseerd. Hieruit kwam naar voren dat het manoeuvreren in een pijp met een helling van 30 graden en het manoeuvreren door een T-bocht problematisch is. Ook de geëiste gemiddelde snelheid van 80 mm/s kan niet worden gehaald. De tekortkomingen van het huidige prototype zijn voor elke module apart geanalyseerd.

De mechanische constructie van de buigmodule is geoptimaliseerd om wrijvingen te verminderen, wat de te behalen klemkracht verhoogde. De theoretisch benodigde klemkracht kan niet worden bepaald omdat de wrijvingscoëfficiënt tussen het wiel en pijppoppervlak te hoog is om te meten. Deze hoge wrijvingscoëfficiënt wordt veroorzaakt door de vervorming van het wielrubber. Het kan wel worden bepaald dat de geleverde klemkracht voldoende is voor de verschillende manoeuvres. De efficiëntie van de buigmodulen is laag, wat mede veroorzaakt wordt door de lage buigsnelheid (14 mm/s). Voor het regelen van de klemkracht, is het beter om de motorstroom te gebruiken voor feedback in plaats van de verdraaiing van de torsieveer. Het voordeel van het gebruiken van de motorstroom voor feedback is dat overbelasting van de motoren kan worden voorkomen. Ook is de klemkoppel spreiding bij een bepaalde motorstroom laag. Een nadeel is dat de buigmotoren niet tegelijk kunnen worden aangestuurd.

Uit de aandrijfmodule analyse kan worden geconcludeerd dat de aandrijfmotoren het benodigde maximale koppel niet kunnen leveren. Dit maximaal benodigd koppel is 131 mNm, terwijl de aandrijfmotoren maar 120 mNm kunnen leveren bij de nominale motorstroom. De efficiëntie van de aandrijfmodulen is ook laag. Dit wordt veroorzaakt door wrijving tussen de tandwielen. De aandrijfsnelheid is ongeveer 70 mm/s bij een koppel van 120 mNm. Omdat ook de buigsnelheid laag is, zal de geëiste gemiddelde snelheid eis van 80 mm/s niet kunnen worden gehaald. Voor autonoom voortbewegen, is het aan te bevelen om een positie/snelheid regeling te combineren met een motorstroom regeling. Dit voorkomt overbelasting van de motoren.

Uit de rotatiemodule analyse kan worden geconcludeerd dat de rotatiemotor het benodigd theoretisch koppel kan leveren. Tijdens de tekortkoming analyse van het huidige prototype, is ook gebleken dat de rotatiemotor ook praktisch het maximaal benodigd koppel kan leveren. Daarom hoeft de rotatiemodule niet te worden geoptimaliseerd.

Nadat alle verschillende modulen zijn geanalyseerd en geoptimaliseerd, zijn de prestaties van het prototype ten opzichte van de gestelde manoeuvreer eisen geëvalueerd. Uit deze evaluatie kan worden geconcludeerd dat de buigmodule optimalisaties de manoeuvreerbaarheid hebben verhoogd. Behalve voor het zijdelings manoeuvreren in een pijp met een helling van 30 graden en de gemiddelde snelheid, kunnen alle andere gestelde manoeuvreer eisen nu worden gehaald. De reden waarom zijdelings een helling van 30 graden niet kan worden opgereden is dat de wielen extra vervormen. Hierdoor is een extra aandrijfkoppel van 40 mNm nodig bovenop het maximum bepaalde aandrijfkoppel. Het aandrijfkoppel kan worden vergroot door de huidige gearbox te vervangen, maar dit heeft als nadeel dat de snelheid dan afneemt. Een meer geschikte oplossing zou zijn om de wrijving, veroorzaakt door het klemmen, te verlagen door het rubber om de wielen te vervangen. Zo kan een betere verhouding tussen de tractie en het aandrijfkoppel worden verkregen.

Preface

With this report I conclude my Master of Science program in Electrical Engineering, which has been a useful addition to my Bachelor education. I would like to thank P. Regtien and E.C. Dertien for their supervising on my work and technical support. I specially would like to thank Tjeerd de Boer for his advice on the report and project planning.

Last but not least, I want to thank my family and girlfriend for their mental support and patience during my study.

Harm de Boer
Enschede, Augustus 2008

Table of contents

1	Introduction.....	8
1.1	Background	8
1.2	The PIRATE Project	8
1.3	Assignment.....	10
1.4	Report Outline	11
2	Pipe Inspection Robot Overview	12
2.1	Break Down of the Prototype.....	12
2.2	Limitations of Current Prototype	13
2.2.1	Driving Horizontally in a Straight Pipe	14
2.2.2	Driving up a Slope of 30°	14
2.2.3	Driving Through a Bend (T-joint/Y-joint)	14
2.2.4	Take a Diameter Change.....	15
2.2.5	Average Speed of 80 mm/s	15
2.2.6	Summary	15
3	Bending Module Analysis	16
3.1	Introduction.....	16
3.2	Basic Bending Module Mechanical Optimizations	17
3.2.1	Motor Housing and Worm Gear Adjustments	17
3.2.2	Wheel Adjustments.....	18
3.2.3	Conclusion	19
3.3	Calibration and Implementation of Clamp Torque Control.....	19
3.3.1	Evaluation of Clamp Torque Control with Torsion Spring	19
3.3.2	Evaluation of Clamp Torque Control with Motor Current Feedback	25
3.3.3	Motor Current Control versus Torsion Spring Control	31
3.4	Theoretical Necessary Clamping Torque	32
3.4.1	Mass Measurements	32
3.4.2	Friction Coefficient Measurements	33
3.4.3	Conclusion	35
3.5	Efficiency and Speed Measurements	35
3.5.1	Efficiency and Speed Test Results	37
3.5.2	Conclusion	39
3.6	Bending Module Conclusion.....	39
4	Driving Module.....	42
4.1	Introduction.....	42
4.2	Necessary Driving Torque	42
4.2.1	Determining the maximum necessary driving torque.....	43
4.2.2	Conclusion	45
4.3	Driving Torque, Efficiency and Speed Measurements.....	46
4.3.1	Driving Torque, Efficiency and Speed test results	46
4.3.2	Conclusion	47
4.4	Driving Module Optimizations.....	47
4.4.1	Gear Train Housing	47
4.4.2	Gearbox	48
4.4.3	Reducing Clamping Torque Friction	48
4.4.4	Driving Control	48
4.5	Driving Module Conclusion.....	49
5	Rotation Module	50
5.1	Introduction.....	50
5.2	Analysis of Current Rotation Module	50
5.3	Rotation Module Conclusion.....	51
6	Conclusions and Recommendations	52
6.1	Requirement Compliance	52

- 6.1.1 Manoeuvring Evaluation52
- 6.2 Recommendations.....53
- Appendix I Test case: Calibration of Clamp Torque Feedback.....56
- Appendix II Test case: Bending and Driving Efficiency66
- Appendix III Test case: Calibration of Motor Current as Clamp Torque Feedback.....72
- Appendix IV Test case: Friction Coefficient.....75
- Appendix V Test case: Maximum Necessary Driving Torque78
- References81

1 Introduction

1.1 Background

The national network of gas mains can be divided into a high-pressure (1-8 bar) network for national distribution stretching 20.000 km and a low pressure network (30 mbar to 100 mbar) for local distribution with a length of roughly 100.000 km. The low-pressure net covers most of the urban area's. Therefore this network has the highest priority with regard to risks for public health and safety. Replacement of pipe sections in an urban area is expensive, so it is important to have accurate data on the locations of leaks and damaged pipe sections. Pipes of gray cast iron and white PVC are most likely to cause leakage. Gray cast iron is especially sensitive to corrosion. PVC is sensitive to point-loads (by tools) and tension (bend, stretch) for example caused by tree roots. The main causes of leakage can be summarized as follows: creep, tension, brittleness, impacts, inferior connections, porous rubber sealing and corrosion. There is another issue with the gas mains, besides pipe leakage: the existing network is not well documented. New sections that have been created in the last decade are well documented, but there is not much information available on older sections in the network. Detailed information possibly never existed or got lost in company merges, takeovers and (computer)system changes.

Currently, the low pressure distribution nets are only inspected by conventional leakage searching above ground. This is a labour-intensive process and does not give any information about layout and quality of the pipe, only leaks that can be 'smelled' can be detected. The accuracy of above ground detection is just several meters. By (Dutch) law, every segment of the gas pipe network has to be inspected every 5 years, but with the current methods this is nearly impossible. High pressure mains are already inspected by robotic systems. These systems are hardly full grown autonomous robots, but more passive data loggers. According to Kiwa Gastec(gas technology research), every year 2000 leaks are being found with the conventional leak inspection methods and 6000 leaks are reported by the public. Continuum (network management branch of Nuon energy company) has had 9000 public leak reports in 2005, from which 1000 were false alarm, 2000 leaks were found in house and 6000 were found in the gas distribution network(see [1]).

1.2 The PIRATE Project

Because of the above mentioned problems with the pipe inspection of low distribution nets, Kiwa Gastec and Continuum contacted the University of Twente in 2006 to find a solution which could improve the quality of inspection of the urban pipe network. In cooperation with DEMCON, a project team was then formed called "Pipe Inspection Robot Autonomous Tube Exploration" (PIRATE). The PIRATE project focuses on the development of an automated system, which can inspect the pipe network from inside the pipe. Goal of the project is to design and build a prototype of an autonomous robot platform, which can navigate through a pipe network.

The design trajectory of the first prototype is shown in figure 1.1. Here, the different trajectory steps are shown with the date at which they were finished.

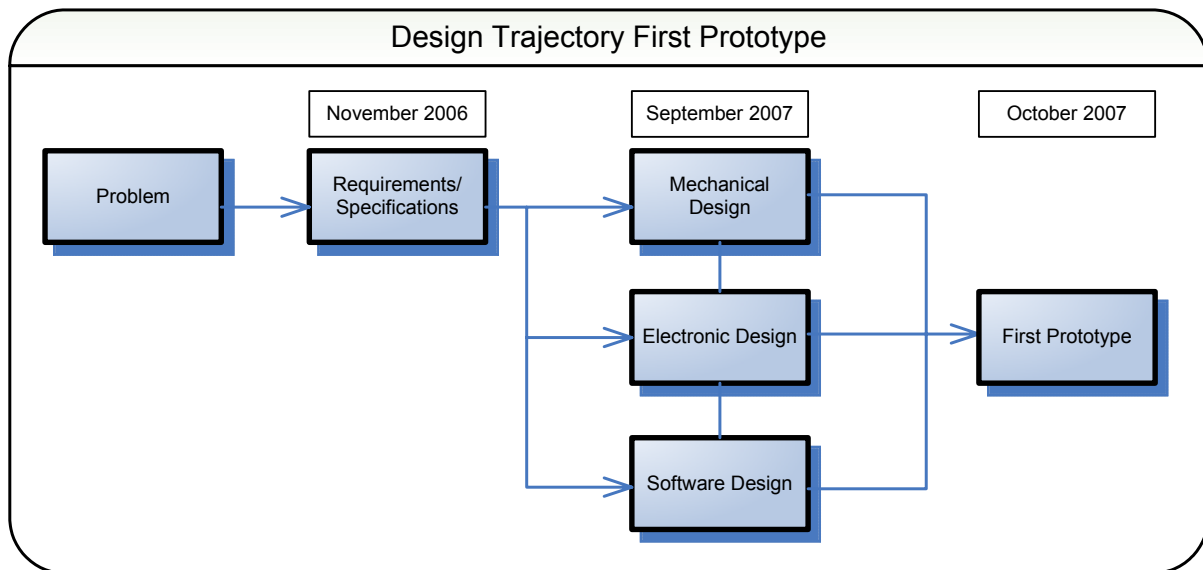


Figure 1.1: First phase design trajectory overview

Because the development of the pipe inspection robot is very challenging, it will be carried out in several phases. Figure 1.1, gives an overview of the executed first phase in the development trajectory. Not all the requirements have to be met in the first phase. For the first phase, the robot should only have to be able to manoeuvre in a pipe network without having to detect leaks and deformations of the gas pipe. The parameters of such a pipe network are shown in table 1.1.

Property	Parameterization
Smallest inner diameter	57 mm.
Biggest inner diameter	119 mm.
Maximum inclination of the pipe	Angle of $\leq 30^\circ$
Gradual diameter change	57 mm. To 119 mm. Angle ranging from 0° to 45°
Bends	Mitered and smooth bends (Angle of $\leq 90^\circ$)

Table 1.1: parameters of the pipe network

Additional requirements on the first phase are:

- The robot should be able to manoeuvre autonomically through a pipe network
- The robot has to communicate wireless with the operator
- Average speed of the robot has to be approximately 80 mm/s
- The robot should have enough power to function for 30 minutes, which should be enough for demonstration purposes.

Not in scope:

- Demands on reliability
- Detections of leaks and deformations of a gas pipe
- Handling of contaminants in the pipe like tar, dust, oil etcetera

These requirements are described more detailed in [1].

The second phase in the design trajectory was the design of the mechanical, electrical and software parts. J.J.G. Vennegoor op Nijhuis finished his Master of Science study at the University of Twente with a thesis about the mechanical design of the pipe inspection prototype. The study translates the specifications and demands of the parties involved in the PIRATE project, to a complete mechanical design. A few mechanical concepts are explored and evaluated on feasibility (see [2]). The chosen concept is further detailed and engineered to a production ready design which is shown in figure 1.2.

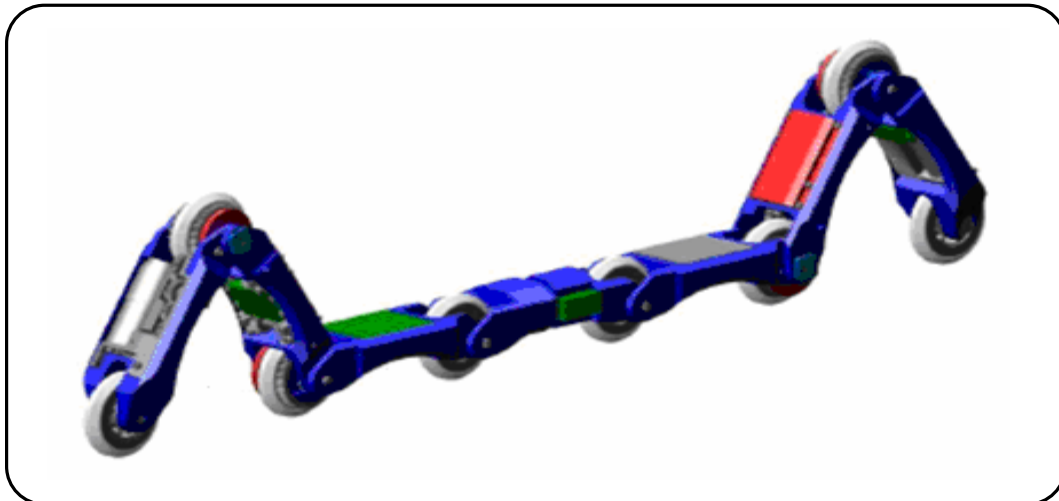


Figure 1.2: The chosen concept

The electronic and software design is divided in two main parts.

- The first part is the design of the local controllers which control all the different motors separately. The design and implementation of these controllers was part of a Master of science internship at the university of Twente which is performed by J. Ansink (see [3]).
- The second part is the main controller which has to control all the routines of the local controller boards and has to communicate with the operator. This is designed and implemented by E.C. Dertien (see [3]).

All these parts combined, resulted in a first prototype of the pipe inspection robot. It has been build for demonstration purposes and to show the technology to the parties involved and potential investors.

1.3 Assignment

The current prototype which has run through two phases of development, does not satisfy all the requirements that it has to fulfil. This master's thesis focuses on a small subset of those requirements e.g. the manoeuvring requirements.

The analysis, optimization and evaluation of the current constructed prototype in relation to the manoeuvring requirements will be described in this report. The shortcomings of the existing prototype in relation to the required manoeuvres, will first be analysed. The current mechanics, electronics and software parts will be evaluated. Possible optimizations will be analysed and implemented or recommended in order to meet the defined specifications. The result of the optimizations on the total prototype will then be evaluated.

1.4 Report Outline

In chapter 2 *Pipe Inspection Overview*, the limitations of the current prototype will be discussed.

In chapter 3, 4 and 5, the different modules of the robot will be evaluated separately. For each module the characteristics are analysed, and possible optimizations are discussed and evaluated.

In chapter 6 *Conclusions and recommendations*, the evaluation of the manoeuvres that can be achieved by the optimized prototype is discussed and recommendations for future development are presented.

2 Pipe Inspection Robot Overview

2.1 Break Down of the Prototype

Figure 2.1 shows schematically the current prototype. It consists of five active modules and two passive modules, each having one of four different specific functions. These modules will be introduced shortly.

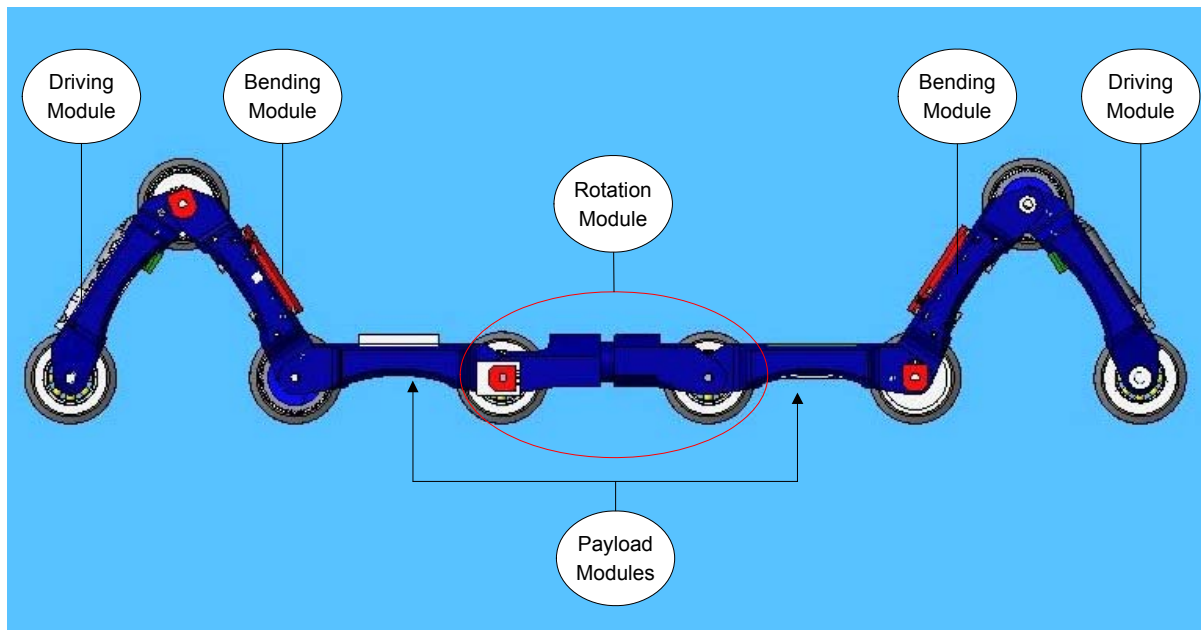


Figure 2.1: Schematic representation of current prototype

- Bending module**
 Two bending modules are present at the rear and front side of the prototype. The function of the bending module is to clamp and orientate the robot in the pipe. The clamping is necessary for providing sufficient traction to the wheels. The bending module is connected to the drive module and to the payload module. The driving module forms together with the bending module the *clamping module*.
- Driving module**
 Two driving modules are present at the rear and front side in the prototype. The function of the driving module is to actuate the robot inside the pipe.
- Rotation module**
 One rotation module is present in the middle of the prototype. The function of the rotation module is to orientate the robot in a different direction. It rotates one half of the robot with respect to the other half.
- Payload modules**
 The two passive payload modules are used to fit the main controller and batteries in the robot.

The electronic infrastructure consists of five local controllers (for each active module) and one main controller, which is schematically shown in figure 2.2.

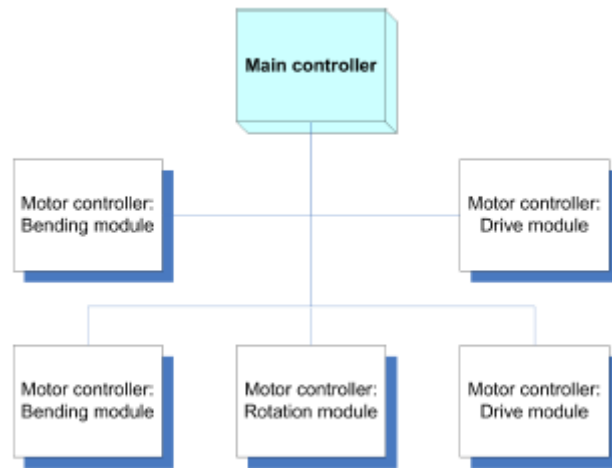


Figure 2.2: schematically overview of electronic infrastructure

The control of the robot is based on distributed control, as can be seen in figure 2.2. The main controller performs the high level control, and the local controllers perform the local feedback control of the different motors for bending, driving and rotating.

The main controller board consists of an ARM7 processor, a 3D acceleration sensor (to determine the orientation of the robot), a memory card slot and a radio module for external (wireless) communication. The current pipe inspection prototype communicates via a RS232 interface with the operator. All the commands of the operator are passed through by the main controller to the different local controllers. The communication between the main controller and the local controllers is based upon I²C.

The local controller consists of an AVR ATmega 168 microcontroller, two H-bridges and sensor interfaces. It provides the following functionalities:

- Control the motors with a PID feedback loop. The feedback consists of information from different sensors. The controller output is a PWM value, which is sent to the H-bridge. When the control loop is disabled, PWM values are sent directly to the H-bridge.
- Analog to digital conversion (ADC) for different sensor interfacing
- Interface for communication with the main controller

More detailed information about the local and main controller can be found in respectively [3] and [4].

2.2 Limitations of Current Prototype

As mentioned in the introduction, the current constructed pipe inspection robot does not meet all the manoeuvring requirements for the first prototype. After performing some small tests with the prototype, the compliance to the following manoeuvring requirements are discussed:

1. Plain driving in horizontally position a straight pipe
2. Driving up a slope of 30°
3. Driving through a bend (T-joint/Y-joint)
4. Take a diameter change
5. Manoeuvring speed

2.2.1 Driving Horizontally in a Straight Pipe

For most of the time, the robot will drive horizontally in a straight pipe. For this manoeuvre, the robot is clamped horizontally inside the pipe by using the rear and front bending module. Both modules are providing the traction to the wheels, which are actuated by the driving modules. The necessary driving and clamping torque for this manoeuvre can be delivered by the modules, so this requirement is met.

2.2.2 Driving up a Slope of 30°

To drive up a slope, it is assumed that the robot will be clamped again horizontally inside the pipe by both bending modules and that the actuation is delivered by both driving modules. For this manoeuvre, the traction force to the wheels has to be larger than for driving in a straight pipe (see [2]). This necessary traction when driving up a slope of 30°, cannot be delivered by the bending modules. The wheels are slipping when they are actuated. This requirement is not met.

2.2.3 Driving Through a Bend (T-joint/Y-joint)

Driving through a bend is a difficult manoeuvre. In figure 2.3 this manoeuvre is schematically shown for a T-joint which is the most difficult.

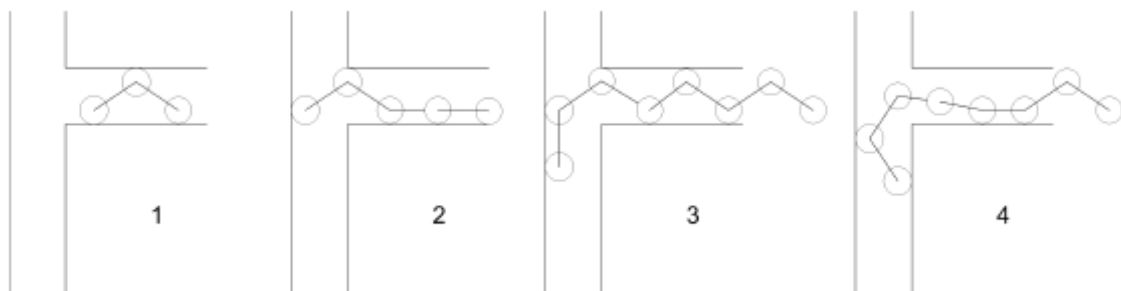


Figure 2.3: Schematic overview of manoeuvring through a T-joint

Figure 2.3 shows a top view of the pipe, where the robot approaches the T-joint driving sideways. The sequence is as follows:

- The robot approaches a T-joint
- After the front driving module has reached the opposite wall, the front actuated wheel loses contact with the wall. The rear module now has to deliver the traction and actuation to push the front module against the opposite wall
- The front module bends into the T-joint and initially builds up traction in the new pipe segment
- As the front module moves further into the new pipe segment, the robot clamps itself again in the new pipe-segment

The delivered clamping torque is insufficient to take these manoeuvres. It cannot provide enough traction when driving sideways and when only one module has to deliver the traction. This part of the requirement is not met.

For approaching the T-joint sideways, the rotation module has to rotate the robot. A rotation sequence includes the following steps:

- First one of the bending elements increases the clamping torque and the other decreases the clamping torque until the wheels lose contact with the wall
- Then the rotation motor turns the required angle

- Now the bending module with the highest clamping torque decreases the torque and the other one increases the torque
- Finally the rotation motor turns to the neutral position

Rotation of the robot inside the pipe is possible with the current prototype. This part of the requirement is met.

2.2.4 Take a Diameter Change

Taking a diameter change does not require specific demands on the delivered torques. The robot should be able to adjust the angle between the driving and bending module while passing through the diameter change, in order to keep the wheels in contact with the wall all the time. With the current prototype, this can be accomplished, so this requirement is met.

2.2.5 Average Speed of 80 mm/s

In all manoeuvres, the average speed should be 80 mm/s. This requirement cannot be met by the current prototype. This was already concluded during the mechanical design (see [2]). This requirement is not met.

2.2.6 Summary

An overview of the evaluation of the current prototype with respect to the manoeuvring requirements, is shown in table 2.1.

Requirement	
Drive horizontally in straight pipe	✓
Rotate the robot	✓
Drive up a slope of 30°	✗
Drive through a bend (T-joint/Y-joint)	✗ ✓
Take a diameter change	✓
Average speed of 80 mm/s	✗

Table 2.1: overview of evaluation

As can be seen in table 2.1, there are three manoeuvring requirements which are not fully met by the first prototype. The shortcomings of the existing prototype in relation to these manoeuvres will be analysed in the next chapters. In these chapters the different active modules will be analysed separately. For each of these modules the characteristics that are lacking will first be analysed. Based on the measurements, the current mechanics, electronics and software parts will be evaluated. Possible optimizations will be analysed and implemented or recommended in order to meet the defined specifications.

3 Bending Module Analysis

3.1 Introduction

In this chapter the analysis of the bending module will be discussed. In the prototype there are two bending modules present as can be seen in figure 2.1. The function of the bending module is to clamp and orientate the robot in the pipe. This clamping is schematically shown in figure 3.1.

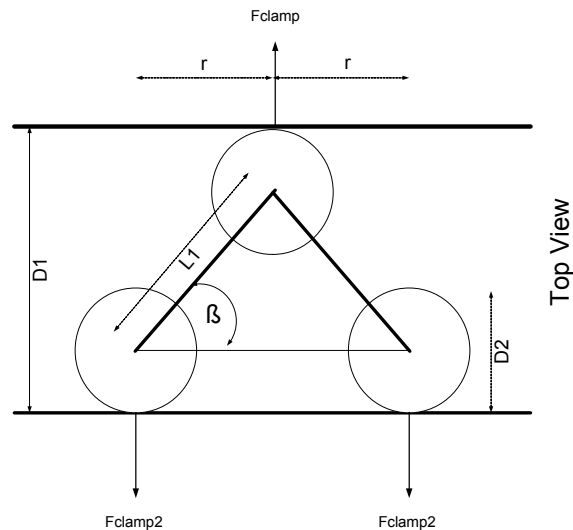


Figure 3.1: Schematic top view of a bending module clamped inside a pipe

Input to the bending module is a Pulse Width Modulated (PWM) signal which controls the power to the bending motors. The bending module contains two Faulhaber 1016 motors to be able to set two bending angles (β) and a torque between the bending module and the two connected modules. With this clamping torque, the robot can clamp itself inside the pipe with a certain clamp force (F_{clamp}). The motors can each deliver a nominal torque of 0.48 mNm. To increase the clamping torque, a transmission gearbox is introduced between the motor and the actuated wheel. The construction of the gearbox is depicted in figure 3.2. With the gearbox a total transmission ratio of 1:5486 with an estimated efficiency of 21% can be reached. This will theoretically provide a clamping torque of 563 mNm at the nominal motor current.



Figure 3.2: Bending module transmission

It is necessary to determine the clamp force provided by the construction in order to understand the characteristics of the bending module. Although position encoders would be ideal for this, they cannot be applied because of the limited space available in the module. Instead the clamping torque force and the different angles are measured with

potentiometers. The potentiometers are connected to a torsion spring element (which is located in the actuated wheels) in order to translate the clamp force to a potentiometer position. Figure 3.3 represents the assembly of the wheels.

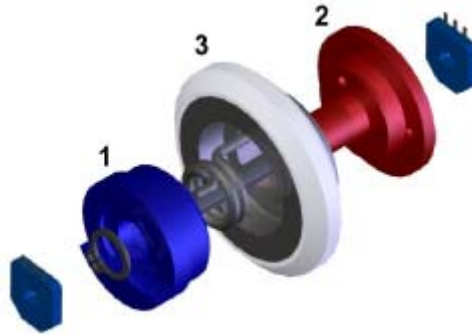


Figure 3.3: Assembly of wheels with torsion spring

This assembly consists of the wheel with a rim and two bodies with a torsion spring in between. The torque applied by the bending module is passed on to body number one and then again transferred to body two via the torsion spring in between body number one and two. Body number two is connected to the adjacent module. If a torque builds up between two modules, the spring will elongate. This elongation is a measure for the build up torque and is measured using a potentiometer that is connected to the shaft of body two and the housing of body one. Finally the two bodies are made out of aluminium bronze to function as sliding bearing for the wheel that surrounds the bodies. The bending angle and clamp force information (potentiometer reading) can be used to control the bending module.

In chapter 2.2 it has been determined that the bending module cannot practically deliver the necessary clamping torque to accomplish the required manoeuvres. To analyse why the bending module cannot deliver the necessary clamping torque, different tests need to be performed to determine the theoretical necessary and the practically delivered clamping torque. After performing some small tests, it has been determined that the bending module suffers a lot from friction. The clamping torque was approximately 20% of what it theoretically could be (563 mNm).

In the following chapters, the different areas of improvement are discussed.

3.2 Basic Bending Module Mechanical Optimizations

Before performing tests on the bending module performance, some basic mechanical imperfections have been addressed. These imperfections are described in the following subchapters.

3.2.1 Motor Housing and Worm Gear Adjustments

The motor housing of the bending module is shown in figure 3.4. In this housing, two motors are placed. As already mentioned, each of these motors is connected to a transmission gearbox. The part directly connected to the motor is a worm gear. This gear is also located in the motor housing. At the end of the worm gear, a bearing has to be connected which fixes the worm gear in the motor housing. However when this bearing is attached, the bending motors suffer from considerable friction. After examining the inside of the motor housing, wear caused by the worm gear could be seen. This indicates that the worm gear and motor housing needs to be adjusted in order to reduce the friction.

After examining the worm gear itself, it could be seen that this gear is assembled with a slight excentricity. It was also noticed that the bearing that is placed at the end of the worm gear has a larger diameter than the motor and worm gear (which have the same diameter). This causes the worm wheel to be pushed extra against the motor housing. By enlarging the diameter by a couple of micrometers at the ends of the motor housing, the motor, worm gear and end bearing can be placed again in a straight line. These optimizations reduce the total amount of friction of the bending module.

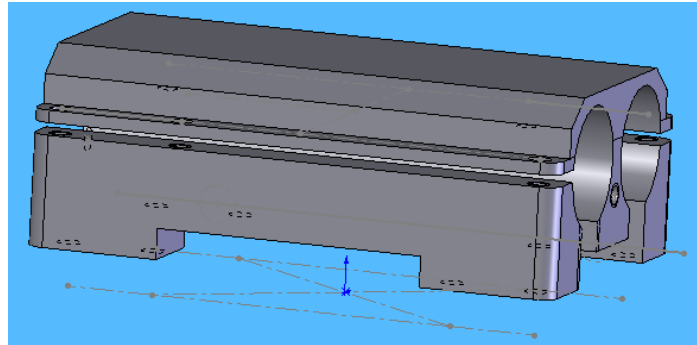


Figure 3.4: Motor housing of the bending module

Besides the mentioned optimizations, the motor housing material (bronze) appears to be not stiff enough. For fixing the bending motors and gears inside the motor housing, screws on the top of the motor housing need to be tightened. However, because the material is not stiff, the motor housing deforms slightly. This makes it difficult to place the motor and gears in a straight line. For this reason it is recommended to choose another material for the motor housing.

3.2.2 Wheel Adjustments

Another part that causes unwanted friction is the actuated wheel. To this wheel, one or two gears are connected which make contact with other gears (from the bending and driving module) as can be seen in figure 3.5 (marked with circles). These gears make also contact with the wheel rubber, which causes additional friction. To eliminate this friction, one millimetre from the sides of the wheel rubber is removed. As can be seen, this adjustment does not decrease the wheel surface which makes contact with the pipe wall.

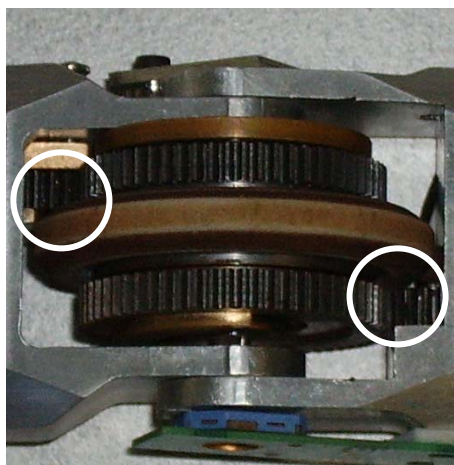


Figure 3.5: Adjusted actuated wheel

Besides the rubber adjustments, also the sliding bearing of the wheels are causing some friction. After adding some oil, these friction are also reduced.

3.2.3 Conclusion

The bending module can theoretically deliver a clamping torque of 563 mNm, but in practice this value is not reached. The bending module is not able to comply to the manoeuvring requirements. Different imperfections of the construction can be pointed out as reason for not reaching the theoretical clamping torque:

- Worm-gear bearing does not fit perfectly in motor housing (friction between worm-gear and motor housing)
- Imperfect attachment worm-gear and motor (slight eccentricity) (friction between worm-gear and motor housing)
- Motor housing deforms when assembled (friction between worm-gear and motor housing)
- Transmission gear contact with wheel rubber (friction between wheel rubber and transmission gear)

Except for the motor housing deformation, all other imperfections have been resolved. The motor housing deformation has not been addressed due to time-constraints. The exact gain in clamping torque due to these improvements has not been determined, but improvements in clamping torque were evident.

The improved construction has been used as basis for further analysis described in this document.

3.3 Calibration and Implementation of Clamp Torque Control

For the different tests that need to be performed, clamping torque control has been implemented and calibrated. Two methods of determining the clamp torque will be discussed.

3.3.1 Evaluation of Clamp Torque Control with Torsion Spring

3.3.1.1 Introduction

As already mentioned in chapter 3.1, the elongation of the torsion spring is a measure for the clamping torque and is measured using a potentiometer. The potentiometer delivers an analogue value which is converted to ADC signals, used as a feedback signal for the clamp torque control.

For the calibration of the clamping torque, two values are relevant:

- The torque per ADC bit (Torque/ADC ratio)
- The ADC value of the bending module when it is not bended (the spring is not elongated in this position)¹

Both values are determined through the clamping torque calibration test, of which the setup is shown in figure 3.6.

¹ In the source code, this value will be used as a “zero point” for the clamp torque feedback

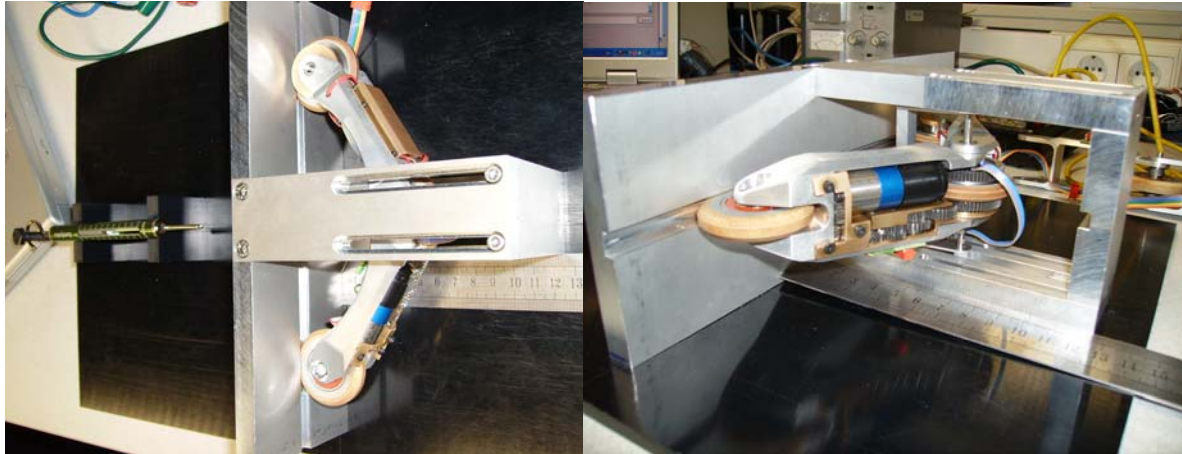


Figure 3.6: test setup for clamp torque calibration

In the figure, the clamping module slides sideways with the middle axis and the lower wheels in a groove, which has the same length as the largest pipe diameter (119 mm). The friction that is caused by this sliding is negligible. For easy calculation, the bending is performed sideways to eliminate the gravitational force. To the bending module, a spring scale is attached to measure the applied clamp force. This spring scale has a range of 0 to 10 Newton. (For more detailed information about the test, see Appendix 1).

The torque/ADC ratio is measured by applying a force of 2 to 8 Newton with steps of 1 Newton. This limited clamp force is necessary to avoid stressing the torsion spring, which can handle a maximum clamp torque of 900 mNm. The ADC values at the different applied clamping forces are read, and the length of the arm of the momentum is measured. This experiment is performed ten times to have a more accurate ADC value. The clamping torque can then be determined with formula (1). Here the applied force is multiplied with the measured arm of the momentum (r):

$$(1) \quad \tau_{clamp} = F_{clamp} \cdot r$$

The torque/ADC ratio can then be determined with formula (2):

$$(2) \quad \tau / ADC \text{ ratio} = \frac{T_n - T_{n+1}}{ADC_n - ADC_{n+1}}$$

Here T_n and ADC_n are for example the clamping torque and ADC measurements for a clamp force of 1 Newton and T_{n+1} and ADC_{n+1} the torque and ADC measurement for a clamp force of 2 Newton. To determine whether after reassembling the clamping module the torque/ADC ratio and setpoint remains the same, the entire experiment is repeated one time after taking apart and reassembling the clamping module.

Besides the Torque/ADC ratio measurements, the ADC value of the bending module at a clamp force of 0 Newton is also measured. This value will be the zero point of the clamping torque feedback.

Because the torsion spring (see chapter 3.1) has a linear characteristic, the Torque/ADC ratio is expected to be approximately constant for all applied clamp forces and is calculated as follows:

According to [3], the angle resolution is calculated with formula (3):

$$(3) \quad \theta_{resolution} = \frac{U_{ref} \cdot \theta_{max}}{U_{in} \cdot bit\ resolution}$$

In this formula, U_{ref} is the reference voltage of the potentiometer (1.1 V, see [3]), U_{in} is the input voltage of the potentiometer (3.3 V, see [3]), θ_{max} is the maximum angle (333°, see [3]) and the bit resolution is 1024 (see [3]). This gives an angle resolution of 0.1084°

According to [2], the maximum torque that the torsion spring can handle (T_{max_spring}) is 900 mNm at a deflection of 24° (θ_{max_spring}). The maximum ADC output can be calculated with formula (4, see [3]), using the angle resolution calculated in the previous step (formula 3):

$$(4) \quad ADC_{max} = \frac{\theta_{max_spring}}{\theta_{resolution}} \approx 221$$

According to [3], the torque/ADC ratio can be determined with formula (5):

$$(5) \quad \tau / ADC\ ratio = \frac{T_{max_spring}}{ADC_{max}} = \frac{900}{221} \approx 4,1\ mNm$$

This means, that one ADC bit should correspond to a clamping torque of 4,1 mNm.

3.3.1.2 Test results

The test results for the front and rear bending module are respectively presented in table 3.1 and 3.2. (More detailed test results can be found in appendix I)

Clamp Force (N)	First measurement		After reassembling	
	μ	σ	μ	σ
2 to 3	4.1	1.2	6.3	1.6
3 to 4	4.1	0.7	3.7	0.8
4 to 5	3.8	0.5	4.2	0.9
5 to 6	5.2	1.5	6.0	2.3
6 to 7	5.0	1.5	19.6	17.9
7 to 8	5.9	1.5	16.6	12.8

Table 3.1: standard deviation and mean of all measured ratio's for the rear bending module

Clamp Force (N)	First measurement		After reassembling	
	μ	σ	μ	σ
2 to 3	4.9	1.5	3.8	0.6
3 to 4	6.3	1.8	4.4	1.2
4 to 5	4.1	0.5	4.0	1.6
5 to 6	4.2	0.3	6.9	4.4
6 to 7	4.1	0.9	4.4	1.3
7 to 8	6.6	3.4	19.4	16.1

Table 3.2: standard deviation and mean of all measured ratio's for the front bending module

In these tables, σ is the standard deviation and μ the mean of all measured Torque/ADC ratio's between two clamp forces. Optimal would be if the mean of the ratio's would be 4,1

and if the standard deviation would be small. As can be seen in table 3.1 and 3.2, the following can be observed:

- there is clearly a non-linear relationship between the applied clamp forces and the measured Torque/ADC ratio's and can vary from 3.7 to 19.6 for increasing clamp forces, which is very large
- there is a spread in the measured Torque/ADC ratio which can get very large. The spread in measured ratio's is smaller for low applied clamp forces than for high applied clamp forces
- the measured Torque/ADC ratio's for both bending modules after reassembling differ a lot

The third observation is due to the impossibility to reassemble the wheel construction exactly in the same position as before the disassembly. For this reason it is not possible to determine a fixed setpoint for the clamp torque feedback.

Both first observations (the non-linear relation and the measured spread in Torque/ADC ratio) are mainly caused by measurement noise, bearing friction and backlash effects that are present in the bending modules.

3.3.1.3 Measurement Noise Effect

To determine the contribution of the measurement noise to the spread in Torque/ADC ratio, a test has been carried out on the ADC value stability. During this test, the motors are active (to create a active/loaded scenario) and the potentiometer is kept at a fixed position (i.e. value does not change). The result is depicted in figure 3.7.

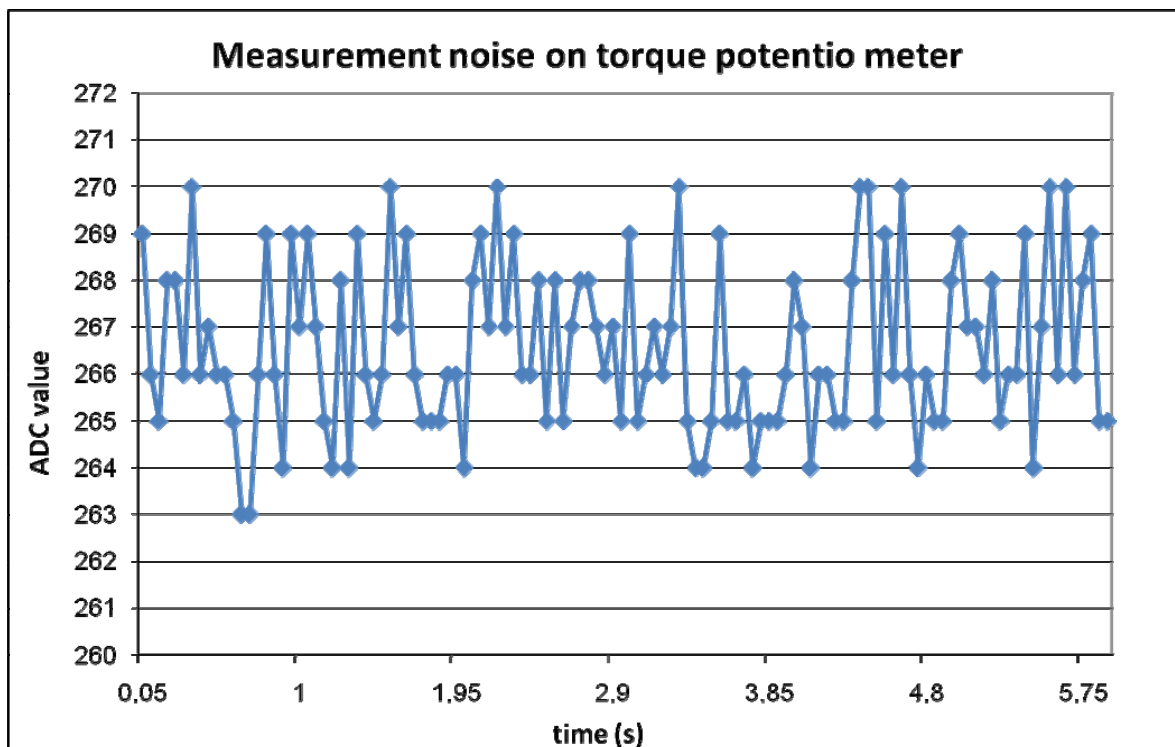


Figure 3.7: Measurement noise on torque potentiometer

In figure 3.7, the ADC values fluctuate considerably as function of time. The fluctuation is around 7 ADC bits (corresponding to an angle of approximately 0.8°), which explains a part

of the measured Torque/ADC ratio spread. This noise does not depend on the state of the motor (active or inactive)

The measurement noise appears to be caused by the max1759 switching regulator, which converts a battery voltage of 3.7V to a voltage of 3.3V. This 3.3V is the input voltage of the potentiometer (U_{in} in formula (3)). Figure 3.8 shows the schematics of this switching regulator.

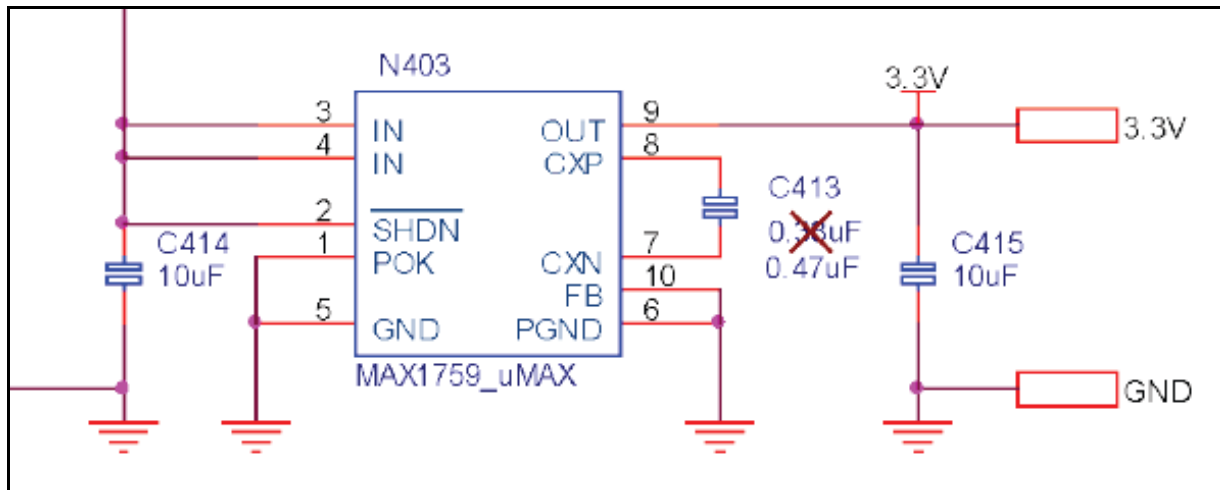


Figure 3.8: Schematic of the max1759 switching regulator

As can be seen in figure 3.8, there is a low pass filter at the output of the switching regulator. This low pass filter is used to produce a smooth output voltage. However, figure 3.9 shows that this output voltage is not stable and has a saw tooth shape.

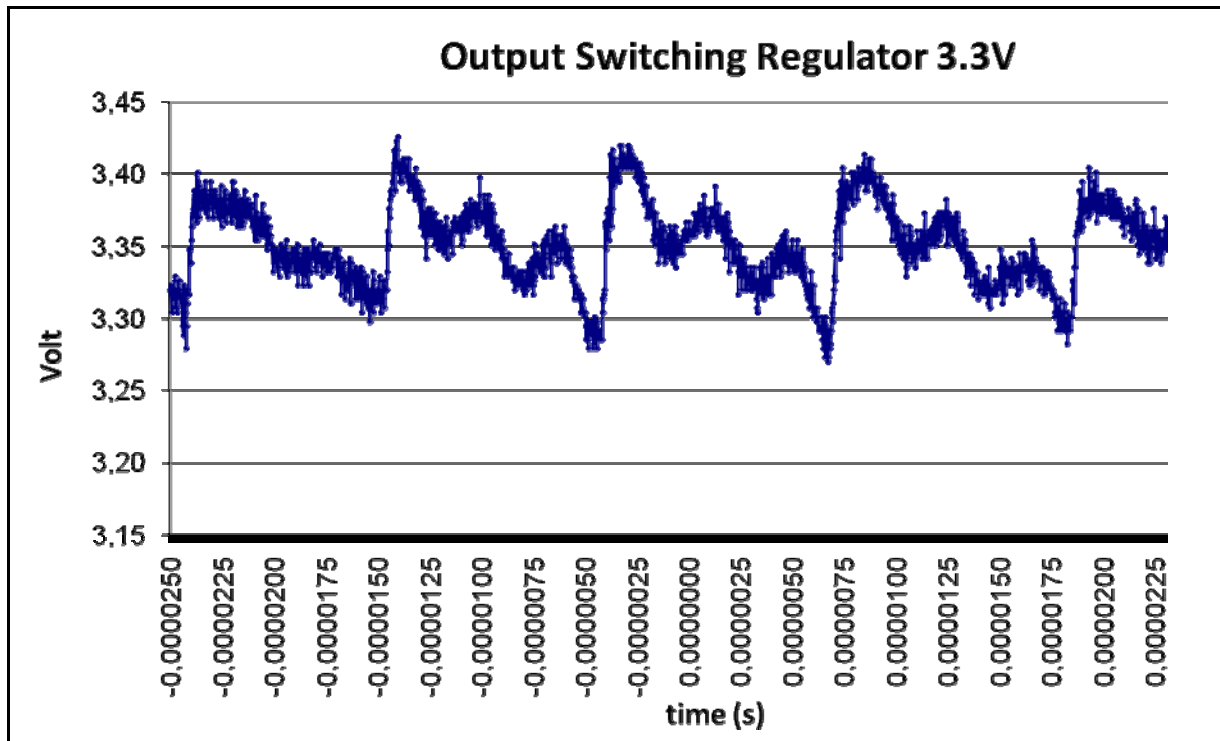


Figure 3.9: Output of the switching regulator

This output voltage of the switching regulator is also used as input voltage for the potentiometers and thereby contributes to the spread in Torque/ADC ratio. To reduce this noise, the low pass filter has to be adjusted such the output voltage is more smooth. From

the current sense amplifier datasheet (see [6]) it is recommended to use 0.33 μF for the C413 capacitor. Because of better availability, currently a 0.47 μF capacitor is used.

3.3.1.4 Bearing Friction Effect

In the actuated wheels of the prototype, a non ideal bearing is used that does not eliminate parasitic friction (friction caused by the different ways the bearing surfaces can rub against each other). Using pre-stressed bearings in the wheel would be a better solution but there is not much space for these bearings. In [2], some experiments were performed with different bearings, but because of the limited space in the wheel and the limited time available, the current bearings are chosen.

This effect contributes to the non-linearity of the torque/ADC ratio.

3.3.1.5 Backlash Effect

The torsion springs in the wheels are not assembled properly. The springs are not centred correctly around the wheel axis as can be seen in figure 3.10. This causes extra friction. Also the spring ends are not well fixed, this causes the backlash present in the bending module. It is difficult to produce torsion springs which do not have any deformation. It is difficult to reshape these springs in the proper form. This effect contributes to the non-linearity in torque/ADC ratio.



Figure 3.10: Torsion spring around wheel axis

3.3.2 Evaluation of Clamp Torque Control with Motor Current Feedback

3.3.2.1 Introduction

As the method for clamping torque determination by torsion spring elongation is not deterministic enough, an alternative method for determining the clamping torque has been considered.

This alternative method uses the motor current to determine the clamp torque. Because there is theoretically a linear relationship between the motor current and the output torque of the Faulhaber motors, this could be a useful torque feedback.

In order to decide whether the motor current can be used to determine the clamp torque, tests have been carried out. The “clamp torque/motor current” characteristic and the spread between measured torques at a certain motor current has to be determined. The test setup is shown in figure 3.11. It consists of a balance and a construction where the “pipe wall” can be simulated with. (For more detailed information see appendix III)

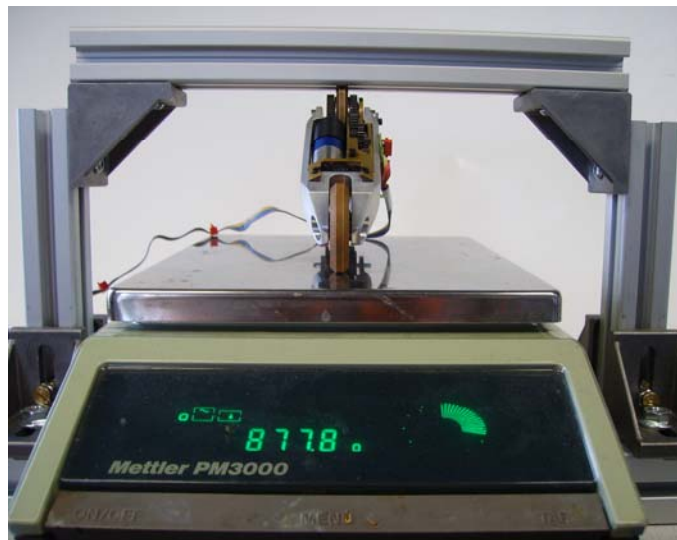


Figure 3.11: test setup

During the test, an external power supply delivers 6 volt to the prototype. For a few motor currents from 0.12 Ampere up to a current of 0.17 Ampere (0.16 Ampere is the nominal current), the clamp torque is measured.

The clamp torque is calculated with formula (6):

$$(6) \quad \tau_{clamp} = m \cdot g \cdot r$$

In formula (6), m is the mass that the balance indicates when the bending module clamps itself at a certain motor current between the balance and “pipe wall”, g is the gravitational acceleration and r the arm of momentum.

3.3.2.2 Test Results

The clamp torque/ motor current characteristic has been determined for the different pipe diameters, because this characteristic will probably differ for different pipe diameters (e.g. 57

mm and 119 mm.). For each motor current at a certain pipe diameter, the achieved clamp torque is measured ten times to determine the clamp torque spread.

Table 3.3 shows the measured mean torques and the standard deviation at the applied motor currents and pipe diameters for the front bending module.

I (Ampere)	Diameter 57 mm.		Diameter 119 mm.	
	μ (mNm)	σ (mNm)	μ (mNm)	σ (mNm)
0.12	508	18	392	36
0.13	548	21	484	32
0.14	569	26	527	20
0.15	613	20	570	18
0.16	622	14	586	13
0.17	628	12	609	13

Table 3.3: measured mean torque and standard deviation of front bending module

Table 3.4 shows the measured mean torques and the standard deviation at the applied motor currents and diameter for the rear bending module.

I (Ampere)	Diameter 57 mm.		Diameter 119 mm.	
	μ (mNm)	σ (mNm)	μ (mNm)	σ (mNm)
0.12	548	13	550	26
0.13	554	12	579	16
0.14	575	9	640	18
0.15	601	10	663	17
0.16	618	12	681	15
0.17	654	12	684	14

Table 3.4: measured mean torque and standard deviation of rear bending module

As can be seen in table 3.3 and 3.4, the following can be observed:

- there is clearly a non-linear relationship between the applied clamp forces and the motor current
- there is a spread in the measured torque as function of the motor current
- there is a difference in the torque/current relation for the different pipe diameters, but not as significant as would have been expected. Expected was that the largest pipe diameter would give the larger torque for the same current. Because the gear that is directly connected to the actuated wheel is assembled with some eccentricity, the front bending module has a larger clamp torque at a smaller diameter.
- it is noticed that both bending modules have a different motor current / clamp torque characteristic. Therefore, the controllers of both modules have to be given separate setpoints to deliver the same clamp torque.

Furthermore, it has been observed that the clamping torque/motor current ratio remains rather constant after disassembling/reassembling of the construction.

3.3.2.3 Complexity of Using Motor Current Feedback

The clamping torque of a bending module is controlled through a PID controller. During the configuration of the PID control, it appeared that there is a lot of noise on the motor current

measurements (as depicted in figure 3.12, where the ADC value represents the motor current).

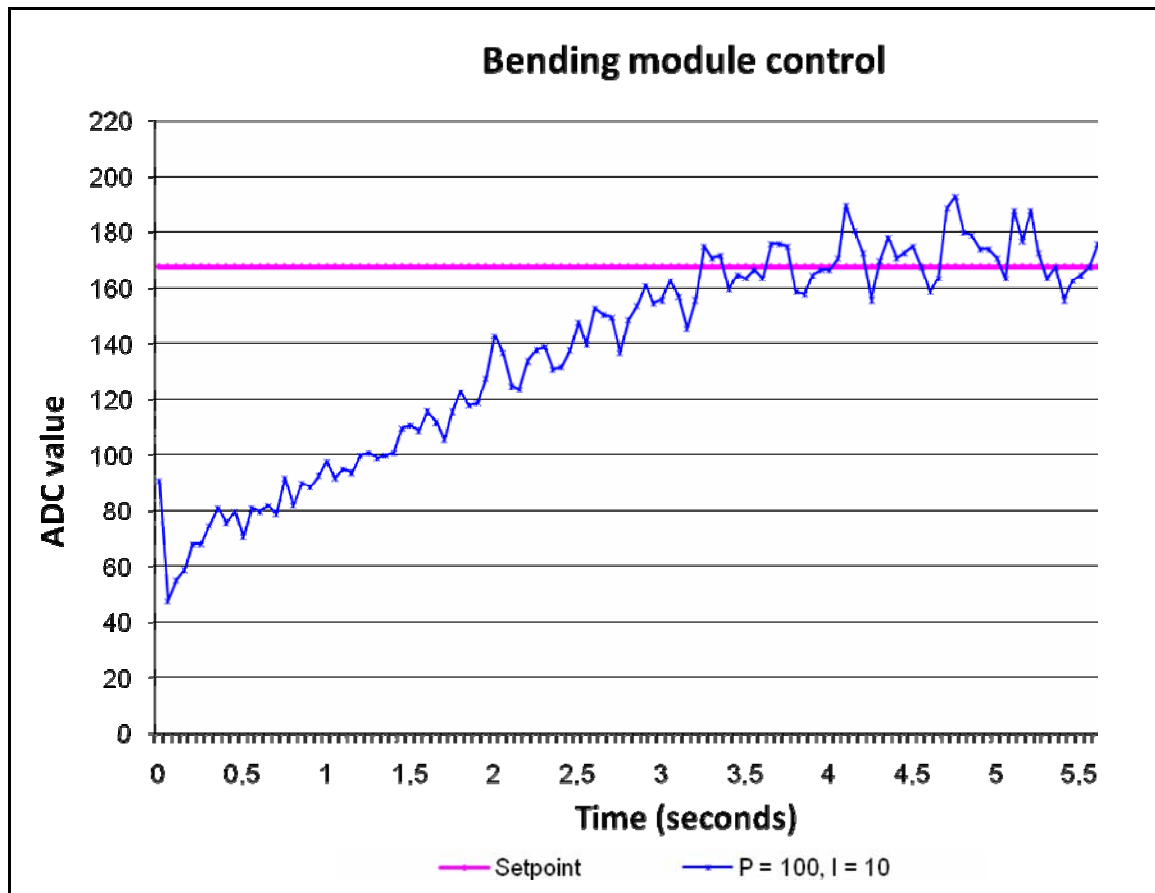


Figure 3.12: Motor current feedback at ADC setpoint of 170

Because the motor current measurement suffers from noise, the PID control will be difficult to configure with the Ziegler and Nichols rules (see [4]), as it is not possible to determine the oscillation frequency, considering only proportional control. Therefore, the PID gains have to be determined experimentally.

Because there is enough damping in the mechanical construction of the prototype, only the proportional and integral action in the PID controller are used. The integral action is used to decrease the stationary error. The PI gains are experimentally tuned to get a smooth step response with minimal overshoot. The PI gains are equal to $K_p = 100$ and $K_i = 10$. Figure 3.12 represents the result of the motor current feedback (ADC value) when the setpoint is 170. Note that in order to have a stable control after reaching the setpoint, a small threshold is implemented in the local controller software to suppress the influence of the measurement noise.

As can be seen in figure 3.12 does the motor feedback control have, besides the first few milliseconds, a more or less smooth step response. In the first few milliseconds a peak motor current is seen as consequence of the motor being started.

To find the cause of this measurement noise, the current sensor interface on the local controller is investigated. Figure 3.13, represents the schematic for the current sensor interface (see also [3]).

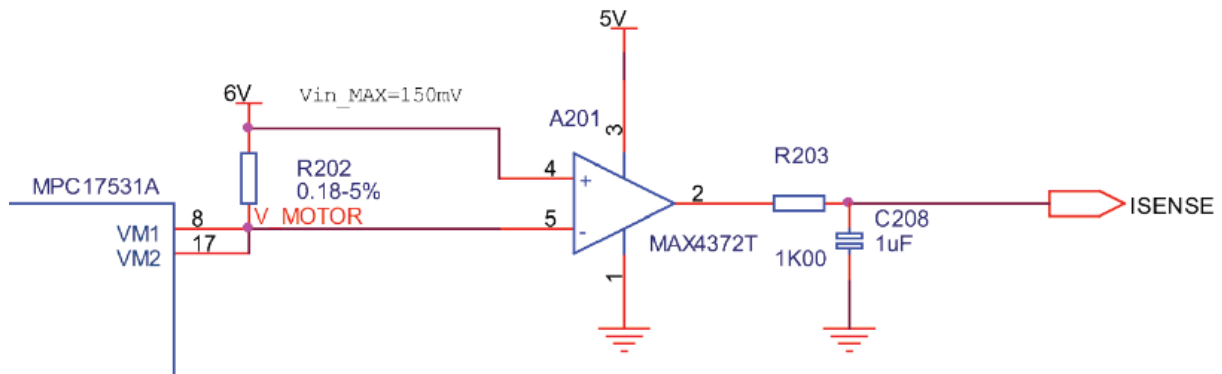


Figure 3.13: high-side current sensing schematic

For the current sensor a high-side current amplifier (MAX4372T) to measure the current at the high-side of the H-bridge is used, because with the H-bridge that is chosen for the local controller it is not possible to do a reliable low-side current sensing. All the current that is used by the motor will flow through the high-side of the bridge without any leakage. To be able to measure the current, a series resistor (R202) is needed that converts the current into a small voltage across the series resistor. This voltage will be amplified with a factor of 20 by the high-side current amplifier and filtered (low pass filter R203 and C208) afterwards to reveal a cleaner voltage for the micro controller AD-converter.

Figure 3.14 and 3.15 shows the measured signal at respectively the high side and low side of resistor R202.

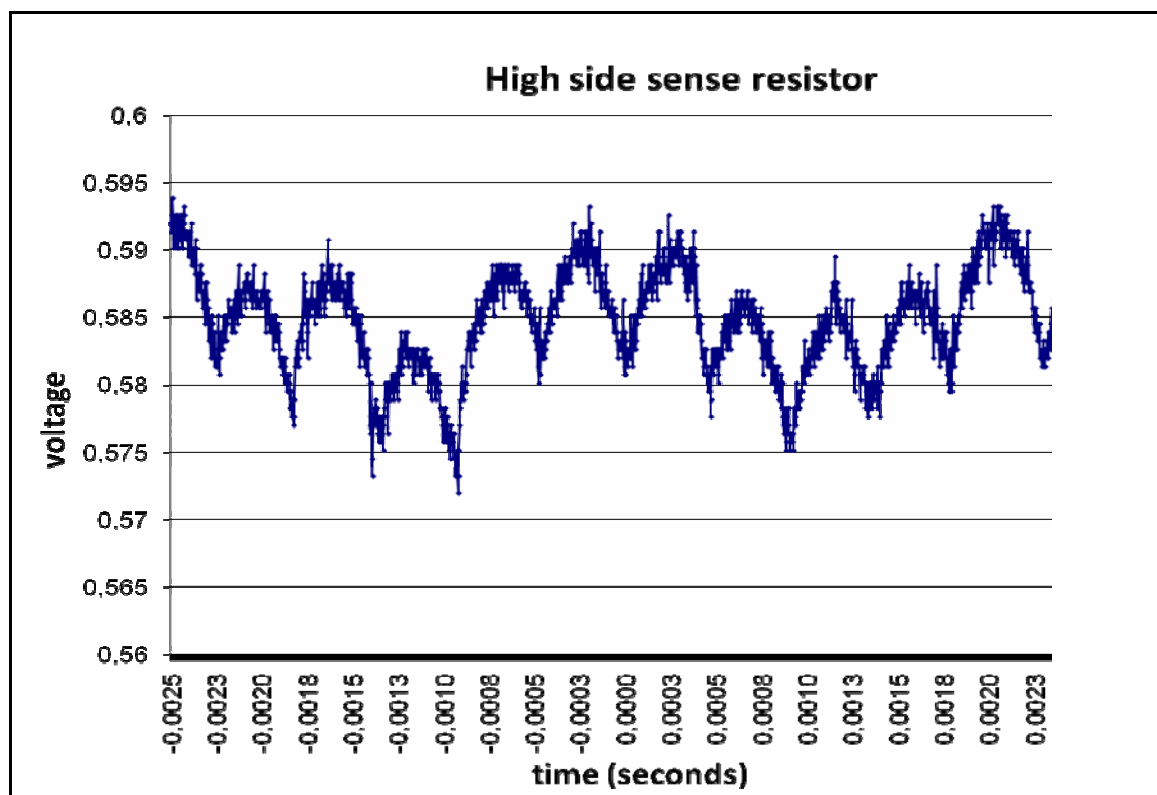


Figure 3.14: Voltage at the high side sense resistor

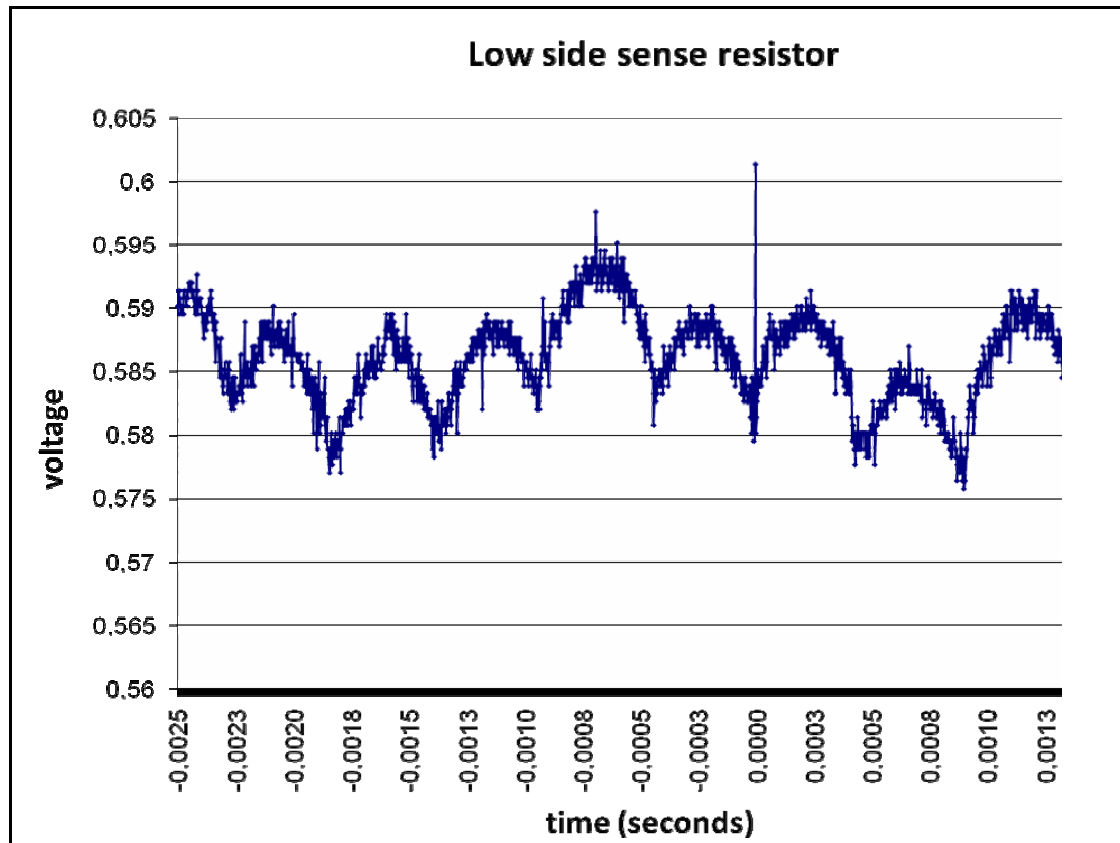


Figure 3.15: Voltage at the low side sense resistor

As can be seen in figure 3.15, the voltage contains besides some noise, a signal. This is likely to be caused by the anchor commutation of the motor because the frequency of this signal depend on the PWM duty cycle. Both the low and high side resistor signals do not differ a lot from each other as expected. The current over the series resistor is than amplified by the current amplifier. The output of this amplifier (with duty cycle of 50%) is shown in figure 3.16.

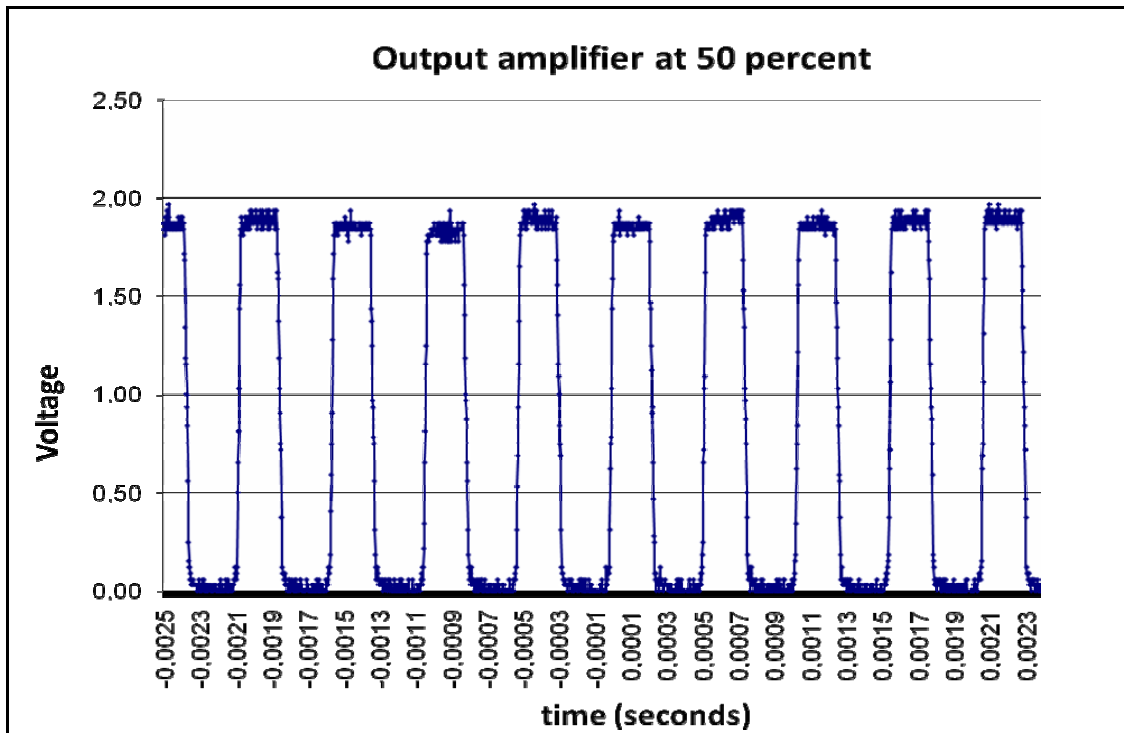


Figure 3.16: Amplifier output at 50% duty cycle

As can be seen in figure 3.16, is the output of the current amplifier a block signal with some small noise. After the filtering a clean voltage is expected, however as can be seen in figure 3.17 has the filtered output voltage a saw tooth shape with a frequency of 2 kHz and a large amplitude of almost 0.3 Volt.

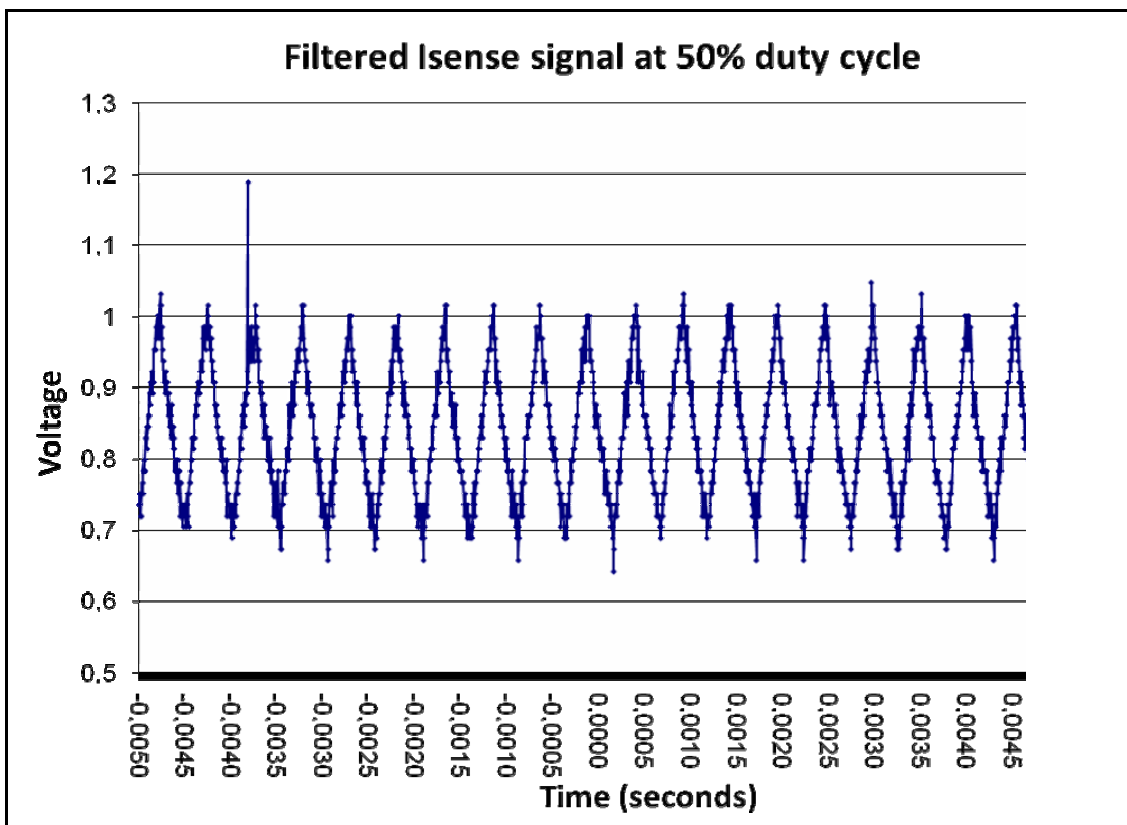


Figure 3.17: Filtered Isense signal at 50% duty cycle

The -3 dB point of the low pass filter is chosen to be approximately 160 Hz. Because the high frequencies are not suppressed enough, this low pass filter has to be adjusted.

This filtered voltage is then send to the AD converter. This explains the noise in the ADC measurements. The motor current measurement noise at 50% and 100% duty cycle after the AD conversion is shown in figure 3.18.

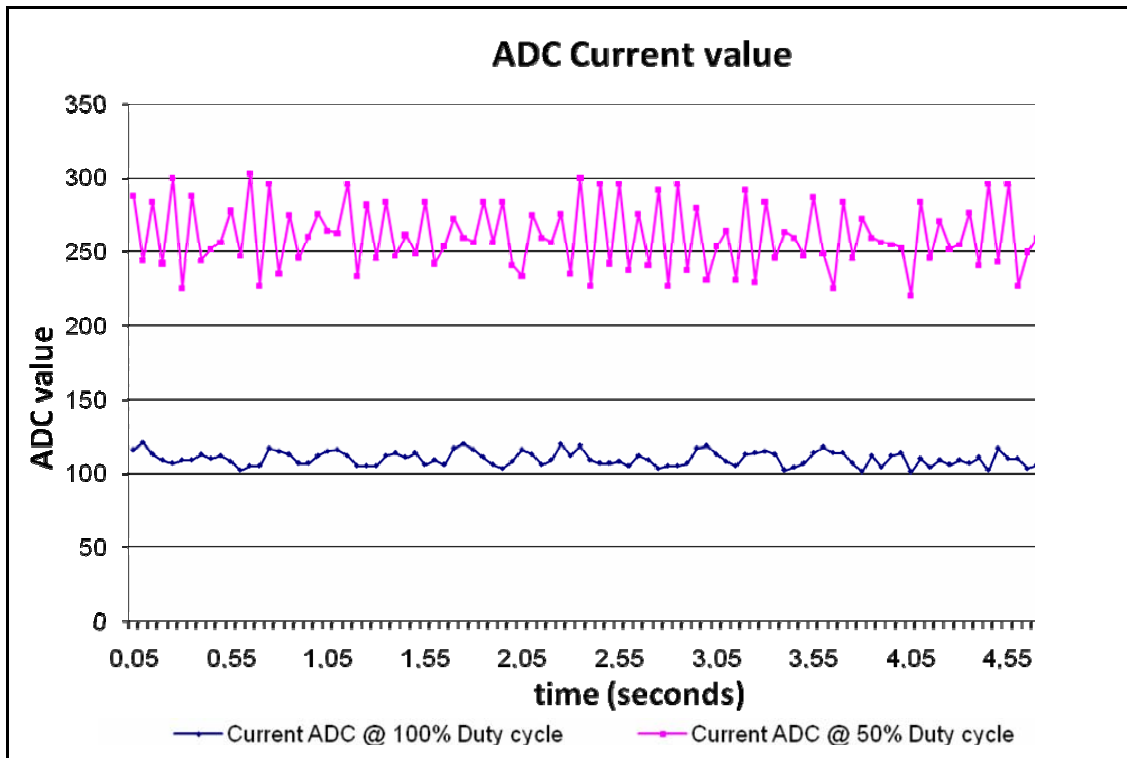


Figure 3.18: Measured ADC motor current value at 50% and 100% duty cyclce

As can be seen in figure 3.18, the maximum measurement noise at 50% is approximately 70 ADC values and for 100% duty cycle 20 ADC values. This corresponds to a motor current of respectively 0.06 and 0.02 Ampere.

3.3.3 Motor Current Control versus Torsion Spring Control

From the evaluation of the torsion spring feedback, it can be concluded that it is difficult to determine the clamping torque through this method:

- the torque/ADC ratio is not constant and has a large spread, caused by mechanical and electrical deficiencies
- the zero reference is not deterministic due to the sensitive assembly of the construction

Using the motor current as clamp torque feedback seems to be a better solution. An advantage of using the motor current for control, is that the zero reference is much more accurate and the deviation of the torque as function of the motor current is low.

An additional advantage of using the motor current method as feedback instead of using the elongation of the torsion spring is that the motor current control prevents excessive stress on the motor. The current prototype method is to prevent stressing the motor by measuring the motor current and limit this motor current. However the motor current is measured for both bending motors at a time. To prevent the motors from being shut down due to the current

limit (high start up motor current), this limit is set high. By only controlling the clamp torque with the elongation of the torsion spring, no care can be taken to prevent the motors from being stressed. By controlling the torque with the motor current, both the torque and the current to the motor is controlled.

A disadvantage of controlling the clamping torque with the motor current, is that just one motor at a time can be used because only the total motor current can be measured. For driving autonomously, also position control (angles that are measured with potentiometers) have to be used in combination with the motor current control. This is because the bending motor that is actuating wheel between the bending module and payload module, will clamp further than required. That is why the position control need to be the high level control. When the position is reached, the bending motor should be shut down.

3.4 Theoretical Necessary Clamping Torque

The theoretically necessary clamping torque will be analysed in this section, in order to determine whether the chosen motors and gears can theoretically deliver this torque. During the detailing of the chosen pipe inspection robot concept, the calculation of the maximum necessary clamping torque is carried out (see [2]).

In the calculations in [2], formula (7) is used for calculating the necessary clamping torque per bending module:

$$(7) \quad \tau_{clamp} = \frac{\frac{1}{8} \cdot m \cdot g}{\mu} \cdot r$$

In this formula represents τ_{clamp} the necessary clamping torque, r a distance called the arm of the momentum (see 3.1), m the mass of the robot, g the gravitational acceleration and μ the friction coefficient between the wheel and the pipe wall. With this formula it has been determined that a clamping torque between 800 and 1000 mNm. should be sufficient for driving in the worst case situation. This worst case situation is estimated to occur when the robot is driving sideways up a slope of 30° in the smallest pipe (57 mm).

This determined necessary clamping torque cannot be provided by the bending motors without stressing them, because they can theoretically deliver only 563 mNm at the nominal motor torque. However, in the necessary clamping torque calculation, estimates of the prototype mass (2.1 Kg) and the friction coefficient (0.3) are used. To be sure that these estimated parameters are justified, the actual mass and friction coefficient of the prototype should be measured because they influence the necessary clamping torque. With these measured parameters, it can be determined if the current motors can theoretically provide the necessary clamping torque.

3.4.1 Mass Measurements

The mass of the prototype that is used in the calculations is 2.1 Kg. However, after weighing the prototype, the mass turns out to be 1.5 Kg. This is a big difference which will influence the total necessary clamping torque.

3.4.2 Friction Coefficient Measurements

Leonardo da Vinci introduced the concept of friction coefficient (μ) as the ratio of the friction force (F_{friction}) divided by the normal load (F_{normal}) (see formula 8):

$$(8) \quad \mu = \frac{F_{\text{friction}}}{F_{\text{normal}}}$$

For low values of the friction coefficient (for instance 0,1), surfaces that are in contact slide more easy than for high friction coefficient values (for instance 1). For the bending module, these surfaces are the wheels and the pipe wall.

In friction, there is a distinction between static and dynamic friction.

In practice, static friction is associated with the “stick” of surfaces that are in contact. The static friction increases with increasing tangential displacement up to the point where the body in contact begins to slide.

Once the bodies in contact are set in motion, a certain force is needed to sustain this motion. This force is the dynamic friction force. The static friction coefficient is typically larger than the dynamic one. Figure 3.19 shows a graph where the typical relation between the friction force and the tangential displacement between two contacting bodies is given.

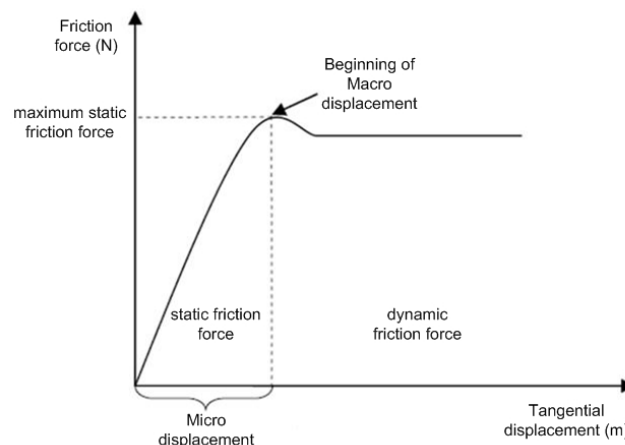


Figure 3.19: typical relation between static and dynamic friction

At a microscopic level, friction is mainly caused by deformation. If one of the contact areas is harder and rougher than the other, the hard one will plough through the soft surface. This deformation can be observed at the rubber wheels of the prototype when the clamping torque increases.

For the friction coefficient measurements, the following is taken into account:

- Besides the static friction coefficient, the dynamic friction coefficient have to be measured too, because it is typically lower than the static one.
- The friction coefficient have to be measured for different clamping torques because the deformation of the wheels influences the measured friction.

The test for determination of the dynamic and static friction coefficient is presented in appendix IV. The test setup is shown in figure 3.20.

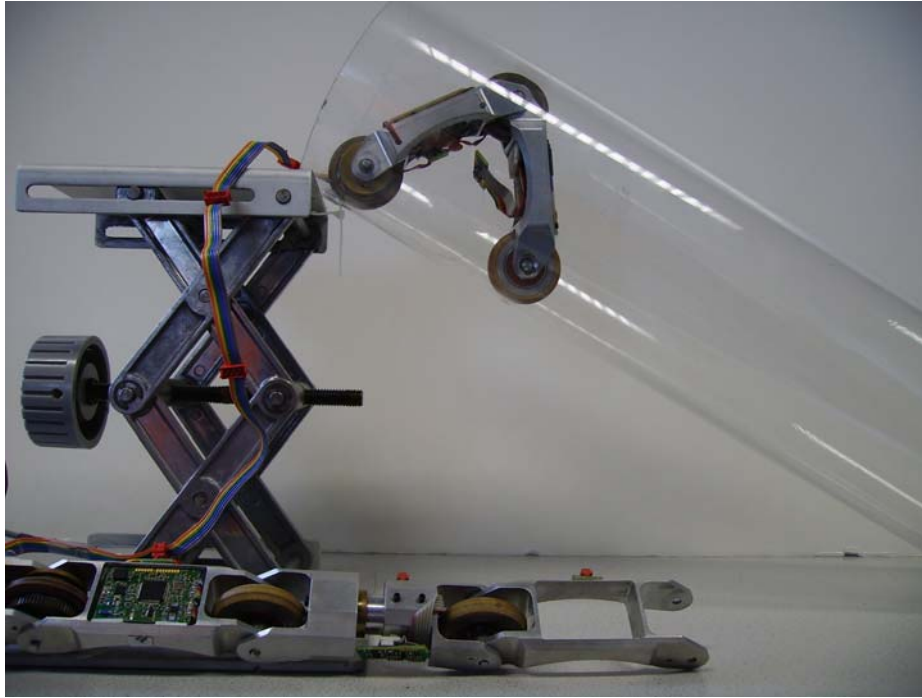


Figure 3.20: test setup

The test setup consists of a bending module which is clamped inside the pipe. The wheels are fixed in this setup, such that they can only slide and not roll. The pipe is connected to a lift, which is used to set a certain angle between the pipe and the table.

First the static friction coefficient is determined by using formula (9):

$$(9) \quad \mu_k = \frac{F_{friction}}{F_{normal}} = \frac{m \cdot g \cdot \sin \theta}{m \cdot g \cdot \cos \theta} = \tan \theta$$

In this formula is m the mass of the bending module, g the gravitational acceleration and θ the inclination angle at which the prototype starts to slide. This sliding angle is determined by enlarging the inclination angle until the robot begins to slide. By using the height of the lift when sliding occurs and the length of the pipe, the sliding angle can be determined.

Because both friction coefficients are influenced by the applied clamp torque, the sliding angle is measured for a few different clamp torques. With these sliding angles, the static friction coefficient is calculated. The measurements are performed in a pipe with a diameter of 119 mm. Here the rear bending module is clamped inside the pipe with a clamp torque of approximately 550 mNm. At this clamp torque, the static friction coefficient cannot be measured because the prototype does not slide even when the angle is 90°. This means that the static friction coefficient is very high and far above the estimated static friction coefficient of 0.5. This estimated static friction coefficient is determined without applying pressure on the rubber wheel (see [2]).

To measure the static friction coefficient, the clamp torque has to be less than 550 mNm. Therefore, the motor current has to be far less than 0.12 Ampere (see 3.3.2.2). The bending motors are less efficient at these low motor current and clamp very slowly, which is not a good solution. Therefore it is pointless to measure the friction coefficient at these low motor currents.

Besides the static friction coefficient, also the dynamic friction coefficient cannot be determined because therefore the prototype has to be in motion. If the prototype is pushed with a certain force, the prototype just slides a small distance.

3.4.3 Conclusion

Neither the static nor dynamic friction coefficient can be measured properly with the proposed test setup because these coefficients are too high. Because the friction coefficient cannot be determined, the theoretical necessary clamp torque for a certain movement cannot be calculated. However, it can be concluded that the necessary clamp torque that the bending modules can deliver is sufficient for the different manoeuvres.

To decide which clamp torque to apply at a certain manoeuvre, the achievable driving torque needs to be known. For the bending module, it would be ideal to operate at the nominal voltage and motor current. However, the torque at this voltage and current could be too high and cause too much friction for the driving module. That is why the decision of determining which clamp torque and speed to apply, has to be weighted with the available driving torque and the necessary driving speed.

3.5 Efficiency and Speed Measurements

To have an indication of the efficiency and the speed of the bending module they are determined at certain motor loads. The test setup is shown in figure 3.23 (for more detailed information see appendix II).

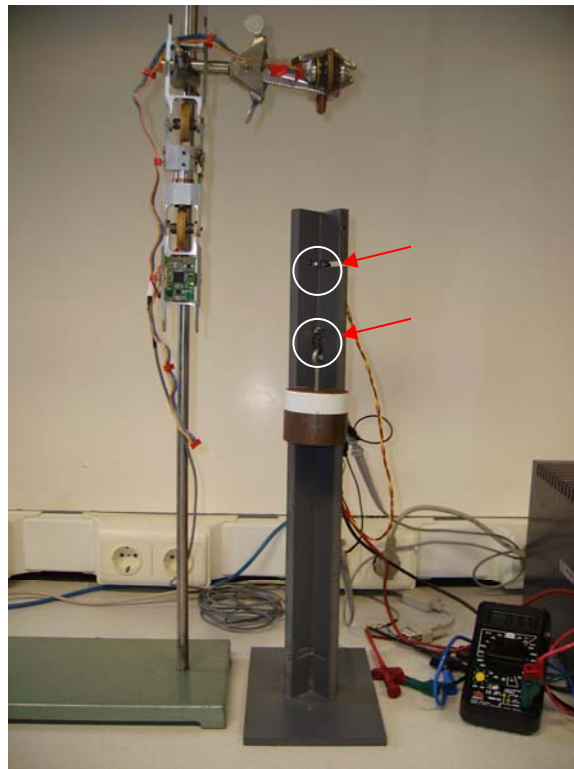


Figure 3.23: test setup

Dependent on the module which is tested, the test setup consist of the bending or driving module which is placed upon a stand. To the actuated wheel, a weight with a certain mass is connected with a wire. This weight slides through a gutter, which contains two photo micro sensors with a distance of 6.5 cm between each other. These sensors are indicated with the

circles in figure 3.21. The efficiency of the bending module is determined by comparing the input power with the output power.

The electrical input power can be calculated with formula (10):

$$(10) \quad P_{in} = U \cdot I$$

In this formula, U is the motor voltage in volts and I the motor current in amperes. The motor voltage and current can be measured with a multi meter.

The mechanical output power can be calculated with formula (11):

$$(11) \quad P_{out} = \tau \cdot \omega$$

Here, τ is the torque in Newton meters and ω the angular velocity in radians per second.

The torque depends on the mass of the connected weight and can be calculated with formula (12):

$$(12) \quad \tau = m \cdot g \cdot r$$

Here, m is the mass of the weight in kilograms, g the gravitational acceleration (9.81) and r the arm of momentum in meters, which is the radius of the actuated wheel were the wire is connected to.

The angular velocity will be determined with the two photo micro sensors and an oscilloscope. If the weight passes a sensor, it will be detected by and the output voltage of the sensor will drop to zero. With the oscilloscope, the time between the voltage drops of both sensors can be determined. The angular velocity, in radians per second, can then be calculated by using formula (13):

$$(13) \quad \omega = \left(\frac{\left(\frac{d}{t} \right)}{2\pi d_2} \right) \cdot 2\pi$$

Here, d is the distance between the two sensors in centimetres and t is the travel time of the weight between the two sensors in seconds and d_2 half the diameter of the actuated wheel in metres.

The efficiency of the motor and gears can be calculated with formula (14):

$$(14) \quad Efficiency = \left(\frac{P_{out}}{P_{in}} \right) \times 100 \%$$

The test has been carried out for a few different applied torques, which can be varied with the mass of the weight. The test has also been performed with direct supplying the power to the motors (nominal voltage) without using the local controller, and with supplying the power by using the local controller in direct PWM mode (without using control). It can then be

determined whether and how the local controller influences the efficiency of the motor and gears.

3.5.1 Efficiency and Speed Test Results

The efficiency and speed measurement results of the bending modules are presented here. Because both the rear and front bending module consists of two motors, four motors are evaluated. To make a distinction between these motors, they are indicated with up and down. The “up” motor is the one that is connected to the wheel which is actuated by the driving motor.

Rear bending module

The efficiency measurement results for the rear bending module “up” are presented in table 3.5 and 3.6.

Torque (mNm)	Motor voltage (V)	Applied Motor Current (A)	Speed (rad/s)	Power in (Watt)	Power out (Watt)	Efficiency
120	6.0	0.07	0.23	0.42	0.03	7%
150	6.0	0.08	0.22	0.48	0.03	7%
180	6.0	0.10	0.20	0.6	0.04	7%

Table 3.5: Efficiency rear up bending module without using local controller

Torque (mNm)	Motor voltage (V)	Applied Motor Current (A)	Speed (rad/s)	Power in (Watt)	Power out (Watt)	Efficiency
120	6	0.06	0.22	0.36	0.026	7%
150	6	0.07	0.20	0.42	0.03	7%
180	5.9	0.10	0.18	0.59	0.03	5%

Table 3.6: Efficiency rear up bending module with using local controller

The efficiency measurement results for the rear bending module “down” are presented in table 3.7 and 3.8.

Torque (mNm)	Motor voltage (V)	Applied Motor Current (A)	Speed (rad/s)	Power in (Watt)	Power out (Watt)	Efficiency
120	6	0.08	0.22	0.48	0.03	6%
150	6	0.10	0.19	0.60	0.29	5%
180	6	0.11	0.18	0.66	0.03	5%

Table 3.7: Efficiency front down bending module without using local controller

Torque (mNm)	Motor voltage (V)	Applied Motor Current (A)	Speed (rad/s)	Power in (Watt)	Power out (Watt)	Efficiency
120	6	0.07	0.20	0.42	0.024	6%
150	5.9	0.09	0.17	0.53	0.026	5%
180	5.9	0.10	0.17	0.59	0.03	5%

Table 3.8: Efficiency front down bending module with using local controller

Front bending module

The efficiency measurement results for the front bending module “up” are presented in table 3.9 and 3.10.

Torque (mNm)	Motor voltage (V)	Applied Motor Current (A)	Speed (rad/s)	Power in (Watt)	Power out (Watt)	Efficiency
120	6	0.08	0.22	0.48	0.026	6%
150	6	0.10	0.18	0.60	0.027	5%
180	6	0.12	0.17	0.72	0.03	4%

Table 3.9: Efficiency front up bending module without using local controller

Torque (mNm)	Motor voltage (V)	Applied Motor Current (A)	Speed (rad/s)	Power in (Watt)	Power out (Watt)	Efficiency
120	5.9	0.08	0.17	0.47	0.023	4%
150	5.9	0.11	0.15	0.65	0.025	3%
180	5.9	0.13	0.14	0.77	0.025	3%

Table 3.10: Efficiency front up bending module with using local controller

The efficiency measurement results for the front bending module “down” are presented in table 3.11 and 3.12.

Torque (mNm)	Motor voltage (V)	Applied Motor Current (A)	Speed (rad/s)	Power in (Watt)	Power out (Watt)	Efficiency
120	6.0	0.06	0.22	0.36	0.026	7%
150	6.0	0.08	0.21	0.48	0.030	7%
180	6.0	0.10	0.19	0.60	0.034	6%

Table 3.11: Efficiency front down bending module without using local controller

Torque (mNm)	Motor voltage (V)	Applied Motor Current (A)	Speed (rad/s)	Power in (Watt)	Power out (Watt)	Efficiency
120	5.9	0.06	0.22	0.35	0.026	7%
150	5.9	0.08	0.19	0.47	0.029	6%
180	5.9	0.09	0.18	0.53	0.032	6%

Table 3.12: Efficiency front down bending module with using local controller

As can be seen from these tables, the efficiencies of these motors and gears are approximately 5% to 7%. For the front up bending module, the efficiency decreases even to 3% to 6%. The extra low efficiency of this motor and gears is caused by the gear that is directly connected to the actuated wheel. The axis of this gear is assembled with some eccentricity.

From the results we can see that for low angular velocities, the efficiency is lower than for high angular velocities. At low velocities the friction is larger, which causes the efficiency to decrease. The maximum measured speed of the bending motors is approximately 0.35 cm/s at a torque of 120 mNm. For larger torques this speed decreases to a measured minimum of 0.21 cm/s at a torque of 180 mNm. At higher torques, this bending speed will decrease even more.

It can also be seen that there is some motor voltage loss when the local controller is used. This is caused by the wire, which is connected between the power supply and the main control board of the robot, and the H-bridge. The wire has a resistance of approximately 1,5

Ω and the H-bridge has an internal resistance of 1.2Ω (see [5]). When the motor current increases, the voltage drop in the wire and the H-bridge increases too. This means that the supplied (nominal) motor voltage has to be increased to compensate for these losses. However the dissipation in the wire is of minor importance in the future, because this wire is not used when the robot is moving autonomously.

3.5.2 Conclusion

From the measurement results of the bending modules, it can be concluded that the efficiencies are very low. These low efficiencies are caused by friction between the gears. The bending speed is approximately 0.21 cm/s and less at clamping torques of 180 mNm . This causes the clamping time to be approximately 6 seconds for pipes with a diameter of 119 mm , this results in a clamping speed of 14 mm/s ($(119 \text{ mm} - 40 \text{ mm}) / 6 \text{ seconds}$). This will decrease the manoeuvring speed of the robot which is required to be approximately 8 cm/s . That is why the low clamping speed has to be compensated by the driving module.

Another important conclusion that can be drawn from this test is that there is a voltage drop in the local controller and the wire between the power supply and the main board of the robot. This loss has to be compensated when supplying voltage to the robot.

3.6 Bending Module Conclusion

From the bending module analysis it can be concluded that after the basic optimizations have been applied (see 3.2), the clamping torque is improved. The clamping torque that can be delivered is higher than is estimated by Jeroen Vennegoor op Nijhuis (see[2])

The maximum necessary clamping torque cannot be theoretically determined, because the friction coefficient between the wheel and pipe wall is too high to measure. This high friction coefficient is caused by the deformation of the wheels. With the results of the friction coefficient test, it can be concluded that the necessary clamp torque that the bending modules can deliver, is sufficient for the different manoeuvres.

The overall efficiency of the bending module is low, which is caused by the low bending speed. This low bending speed needs to be compensated by the driving module to fulfil the required manoeuvring speed of 8 cm/s . For the front up bending module, the efficiency is the lowest. The extra low efficiency of this motor and gears is caused by the gear that is directly connected to the actuated wheel. The axis of this gear is assembled with some eccentricity and needs to be adjusted.

There is also a voltage drop in the local controller and the wire between the power supply and the main board of the robot. This loss has to be compensated when supplying voltage to the prototype. However, the voltage drop in the wire is of minor importance in the future, because this wire is not used when the robot is moving autonomously.

The clamping torque which is applied against the wall needs to be controlled. To determine the clamping torque the torsion spring elongation cannot be used because the torque/ADC ratio is non linear. There is a large spread in measured torque/ADC values which is caused by mechanical and electrical parts. The mechanical part that causes this spread is the actuated wheel. The sliding bearing in these wheels does not eliminate parasitic friction. Also the torsion springs in the wheels are deformed and are not assembled properly. The electronic part that is also causing the measured spread in torque/ADC ratio is the switching regulator. This switching regulator causes some noise on the ADC measurements.

Using the motor current as clamp torque feedback seems to be a better solution. An advantage of using the motor current for control, is that stressing of the motors is prevented. A disadvantage is that only one motor at a time can be used. Also the zero reference is much more accurate and the deviation of the torque as function of the motor current is low.

The motor current control is difficult to configure because there is a lot of measurement noise. This measurement noise is caused by the low pass filter at the output of the high-side current amplifier (MAX4372T) which has to be adjusted.

4 Driving Module

4.1 Introduction

In this chapter, the analysis of the driving module will be discussed. In the prototype, there are two bending module present as can be seen in figure 2.1. The function of the driving module is to actuate the robot. Figure 4.1 shows the drive module. As can be seen, each drive module contain only one motor because of the limited dimensions. This motor is the Faulhaber 1717, which drives the wheel that is located between the drive and the bending module. This wheel is driven because on this wheel, the largest normal force is exerted. This means that this wheel has the largest traction.



Figure 4.1: Schematic view of the driving module

The transmission between the drive motor and the wheel consists of a small gearbox and multiple gears as can be seen in figure 4.2. These reductions are necessary to provide a higher driving torque. The total reduction is 1:168.66 with an estimated efficiency of 38%. This will theoretically provide a clamp torque of 157 mNm. at the nominal motor current.



Figure 4.2: Driving module transmission

To the motor, an incremental encoder is connected. This encoder is added to create a position or velocity feedback loop to compensate for variations in the output variables that are influenced by the environment.

4.2 Necessary Driving Torque

The analysis of the driving module starts with calculating the necessary driving torque that has to be provided by the motors. During the detailing of the chosen pipe inspection robot concept, the calculation of the necessary driving torque is carried out. (see [2]). From this calculation follows that a driving torque of 100 mNm. should be sufficient for driving in the worst case scenario. This worst case scenario is assumed to occur when the robot is driving sideways up a slope of 30 degrees in the smallest pipe. This means that the driving motors can deliver sufficient driving torque. In this calculation however, the friction that the robot has to overcome, are rough estimates. To be sure that the chosen motors can provide the necessary torque, it is important to recalculate the necessary driving torque. For this

recalculation, the friction that the robot has to overcome in the worst case situation, have to be determined.

4.2.1 Determining the maximum necessary driving torque

Theoretically determining the maximum necessary driving torque is difficult, because there are lots of different friction present in the robot. This friction also depend on the applied clamping torque. To get an approximation of the friction forces at different manoeuvres, tests have been performed. Also the extra clamping torque caused by the reaction torque of the driving module itself (see [2]), is experimentally determined.

The test setup is shown in figure 4.3. For more detailed information see appendix V.

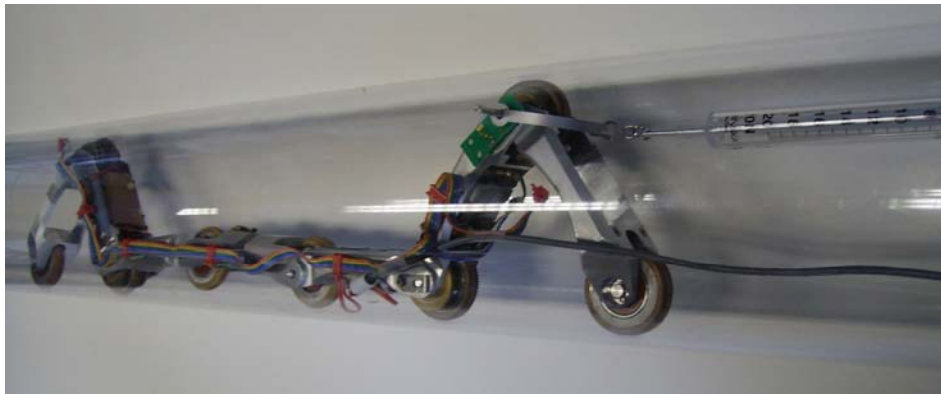


Figure 4.3: test setup

First the friction caused by the clamping torque and rolling friction is determined for the different manoeuvres. These manoeuvres are:

- 1) One bending module clamps itself horizontal in the pipe (for the rear and front bending module)
- 2) Two bending modules clamp together horizontally in the pipe
- 3) Two bending modules clamping sideways in the pipe
- 4) Two bending modules clamping sideways in the pipe and driving up a slope of 30°

For all of these manoeuvres, a pipe with a diameter of 119 mm. is used, because here the highest clamping torques are achieved. Also the driving motors are removed, to rule out friction that are caused by the gears of the driving module.

The clamping is performed for motor currents from 0.12 Ampere to 0.17 Ampere. The friction is measured with a spring scale, which is attached to the bending module. This can be seen in figure 4.3. The force where the wheels begin to turn, is the friction force. These friction forces are determined 5 times to have a more accurate approximation.

Secondly, the extra clamping torque caused by the reaction torque of the driving module itself, will experimentally be determined. This is done by clamping one bending module inside the pipe with the driving motor reattached. The spring scale will also be attached to the bending module. Then the driving force is measured with the spring scale, when the robot is moving forward and when it is moving backwards. The half of the difference between these two driving forces is approximately the extra friction caused by the driving direction.

The maximum necessary driving torque is then calculated with formula (15):

$$(15) \quad \tau_{drive} = F_{max} \cdot r$$

In this formula is F_{max} the maximum friction force that the driving modules have to overcome and r the arm of the momentum. This arm is equal to the radius of the wheel, which is 0.02 meter.

Besides the already mentioned manoeuvres, the manoeuvre where the two bending modules clamp sideways in the pipe under a slope of 30° is determined theoretically. This is determined theoretically because it is difficult to measure with the proposed test setup.

The measured friction caused by the clamping torque and the rolling friction are presented in table 4.1 to 4.4. In this tables, the measured mean friction force and the standard deviation are given.

I (A)	0.12	0.13	0.14	0.15	0.16	0.17
Mean (N)	2.8	3	3.1	3.1	3.2	3.2
σ (N)	0.16	0.21	0.07	0.1	0.04	0.05

Table 4.1: Friction measured for manoeuvre 1 with front bending module

I (A)	0.12	0.13	0.14	0.15	0.16	0.17
Mean (N)	3	3.1	3.1	3.2	3.2	3.3
σ (N)	0.07	0.06	0.06	0.06	0.07	0.04

Table 4.2: Friction measured for manoeuvre 1 with rear bending module

I (A)	0.13	0.15	0.17
Mean (N)	4.1	4.2	4.3
σ (N)	0.13	0.05	0.11

Table 4.3: Friction measured for manoeuvre 2

I (A)	0.13	0.15	0.17
Mean (N)	4.5	4.6	4.7
σ (N)	0.12	0.19	0.07

Table 4.4: Friction measured for manoeuvre 3

From the bending module analysis, we know that there is a spread in clamping torques at the different motor currents. However, as can be seen in table 4.1 and 4.2, there are no big differences in measured friction for the different motor currents. The friction depends for a large part on the deformation of the wheel rubber. To increase the deformation of this rubber, the clamp torque has to increase. At a large deformation, the elasticity of the rubber will decrease and relatively more clamp torque has to be applied to deform the rubber. This explains the small difference in friction forces and the small increase in friction force at higher clamp torques. The maximum measured standard deviation is 0.21 Newton, which means that the spread in measured friction forces is small. The maximum measured difference in friction force is 0.5 Newton.

Because the friction force differs not much between applied motor currents, the friction force for manoeuvre 2 and 3 are only measured for 3 motor currents. These friction forces have to be overcome by both driving modules. This means that the friction for manoeuvre 2 and 3 per driving module is less high than for manoeuvre 1. We can also observe a difference between the friction force when driving horizontally in the pipe and driving sideways in the pipe. This is caused by the different deformation of the rubber wheels. The maximum

measured standard deviation is for these two manoeuvres 0.19 Newton. Also here the maximum measured difference in friction force is 0.5 Newton.

Also the extra clamping torque caused by the reaction torque of the driving module itself, is experimentally determined. Table 4.5 presents the measurement results.

I (A)	0.7	0.8	0.9
Torque(N)	0.3	0.35	0.4

Table 4.5: Extra clamping torque caused by the reaction torque

As can be seen is the extra clamping torque approximately 0.3 Newton at a motor current of 0.7 Ampere. This needs to be added or subtracted (depends on the driving direction) to the friction forces determined in the measurements where just one module actuates the robot. When two driving modules are used, this extra friction force is added to the front and subtracted from the rear driving module, or vice versa. This cancels the extra friction.

For manoeuvre 4, the necessary driving torque is the highest per driving module. This is because some extra torque needs to be applied to “push” the robot up the slope. This extra torque can be calculated with formula 16:

$$(16) \quad \tau_{push} = m \cdot g \cdot \sin(\alpha) \cdot r$$

In this formula is m the mass of the robot (1.5 kg.), g the gravitational acceleration (9.8 m/s), α the slope (30°) and r the arm of momentum (0.02 m). The total ‘push’ torque at 30° is almost 147 mNm. Per motor, an extra torque of approximately 74 mNm has to be delivered.

4.2.2 Conclusion

The necessary driving torque per manoeuvre is summarized in table 4.6. For all manoeuvres, an extra torque of 10 mNm is added to compensate the maximum measured difference in friction forces. For manoeuvre 1, the extra clamp torque caused by the reaction force is also added. The driving torque for manoeuvre 4 is calculated by adding the “push” torque to the calculated driving torque for manoeuvre 3.

Manoeuvre	Motor current (Ampere)		
	0.13	0.15	0.17
	Driving torque (mNm)		
1	78	82	84
2	51	52	53
3	55	56	57
4	129	130	131

Table 4.6: Maximum driving torque for each manoeuvre

As can be seen in table 4.6, the maximum necessary driving torque is approximately 131 mNm. This maximum necessary driving torque needs to be applied when the pipe inspection robot is driving up a slope of 30° sideways in the largest pipe. In the following section it will be determined if the driving motors can practically deliver the maximum driving torque.

4.3 Driving Torque, Efficiency and Speed Measurements

To have an indication of the efficiency and the speed of the bending module they are determined at certain motor loads. The test setup is the same as for the bending module and is shown in figure 3.23. The test will also be performed with direct supplying the power to the motors (nominal voltage) without using the local controller, and with supplying the power by using the local controller in direct PWM mode (without using control). It can then be decided if the local controller influences the efficiency of the motor and gears.

4.3.1 Driving Torque, Efficiency and Speed test results

The robot consists of two driving modules, each containing one motor. Both the rear and front driving motors and gears motors are evaluated.

Front driving module

The efficiency measurement results for the front driving module are presented in table 4.7 and 4.8.

Torque (mNm)	Motor voltage (V)	Applied Motor Current (A)	Speed (rad/s)	Power in (Watt)	Power out (Watt)	Efficiency
66	5.3	0.29	5.4	1.54	0.36	23%
96	4.9	0.40	4.3	1.96	0.41	21%
120	-	-	-	-	-	-

Table 4.7: Efficiency front driving module without using local controller

Torque (mNm)	Motor voltage (V)	Applied Motor Current (A)	Speed (rad/s)	Power in (Watt)	Power out (Watt)	Efficiency
66	6	0.29	6.2	1.74	0.41	24%
96	6	0.39	5.4	2.34	0.52	22%
120	6	0.50	5.4	3.00	0.65	22%

Table 4.8: Efficiency front driving module with using local controller

Rear driving module

The efficiency measurement results for the rear driving module are presented in table 4.9 and 4.10.

Torque (mNm)	Motor voltage (V)	Applied Motor Current (A)	Speed (rad/s)	Power in (Watt)	Power out (Watt)	Efficiency
66	6	0.31	6.2	1.86	0.41	22%
96	6	0.44	5.4	2.64	0.52	20%
120	6	0.55	4.9	3.3	0.59	18%

Table 4.9: Efficiency rear driving module without using local controller

Torque (mNm)	Motor voltage (V)	Applied Motor Current (A)	Speed (rad/s)	Power in (Watt)	Power out (Watt)	Efficiency
66	5	0.31	4.8	1.55	0.32	21%
96	4.6	0.46	4.3	2.12	0.41	20%
120	-	-	-	-	-	-

Table 4.10: Efficiency rear driving module with using local controller

As can be seen from the efficiency measurement results of both driving modules, the efficiency of the motor and gears are approximately 18% to 24%. Also for the driving module the efficiency is higher at higher angular velocities. The maximum measured speed of the driving motors is approximately 9 cm/s at a torque of 66 mNm. For larger torques this speed decreases to a measured minimum of approximately 7 cm/s at the nominal motor current (0.50A).

It can also be noticed that the voltage losses when using the local controller are larger for the driving module than for the bending module. This is caused by the higher applied motor currents. At a torque of 120 mNm this voltage loss is decreased to such an extent that the weight cannot be lifted anymore and no efficiency can be measured. This voltage losses have to be taken into account when supplying voltage to the robot.

4.3.2 Conclusion

From the measurement results of the driving modules, it can be concluded that the efficiencies are very low. These low efficiencies are caused by friction between the gears. The driving speed is approximately 7 cm/s and less above driving torques of 120 mNm. This is less than the required manoeuvring speed of 8 cm/s. Because the bending speed is also low, the required manoeuvring speed cannot be supplied.

The same conclusion as for the bending module can be drawn about the occurring voltage drop in the local controller and the wire between the power supply and the main board of the robot. For the driving module this can get large (1.1 volt at 0.50 Ampere). This loss has to be compensated when supplying voltage to the robot.

From this test, also the driving torque at the nominal motor current (0.50 Ampere) can be determined. This driving torque is approximately 120 mNm. From the necessary driving torque test described in the previous section, a maximum driving torque of 131 mNm is determined. This means that the driving motors cannot deliver the necessary maximum torque without stressing the motors. This is not recommendable, and that is why the driving motors have to be replaced or that the friction have to be reduced. Recommendations for optimizing the bending module are presented in the following section.

4.4 Driving Module Optimizations

Recommendations for optimizing the driving module, are discussed in this section. These parts are the gear train housing and the gearbox. Also recommendations for decreasing the friction caused by the clamping torque and for controlling the driving motor will be presented.

4.4.1 Gear Train Housing

From the efficiency test that has been performed, it can be seen that the efficiency of the rear driving module is lower than the front driving module. After examining both driving modules, it is determined that the gear train of the rear driving module is assembled with a slight eccentricity. The assembled gear train of both the driving modules are shown in figure 4.4. On the left, the rear driving module is shown. This eccentric assembled gear train, cause the gears of the driving module to make bad contact with the gear that is attached to the wheel. Also the wheel rubber makes some slight contact with the gear housing of the rear module, which causes additional friction. This gear train needs to be reconstructed, to increase the efficiency of the rear driving module.

A general recommendation for both driving modules, is to replace the peg that fixates the gear train by a screw. The peg can slide easily out the module, because it cannot stick enough to the gear train. This peg can be seen in figure 4.4.

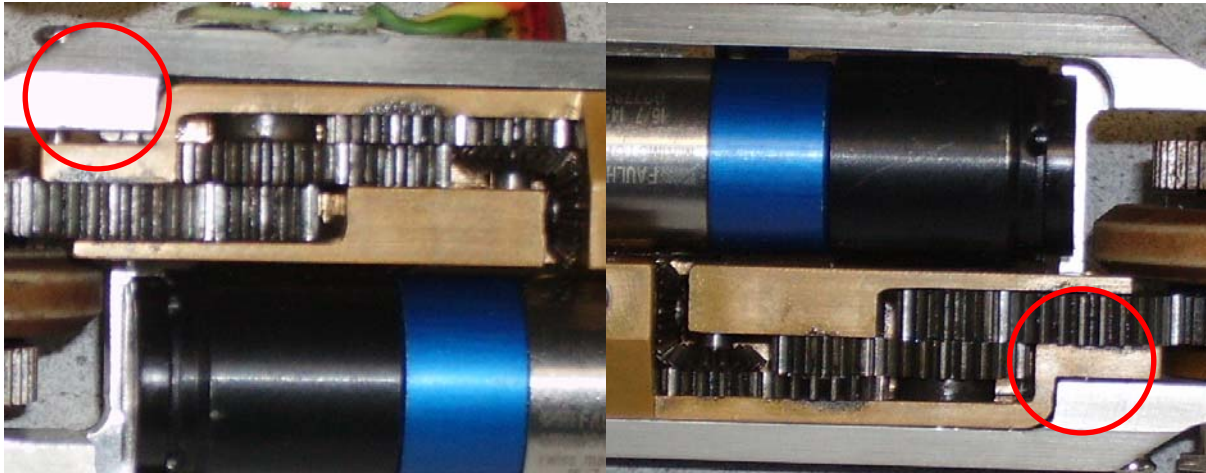


Figure 4.4: gear train of the rear and front driving module

4.3.2 Gearbox

To increase the driving torque, some research has been done to find another motor and gearbox. It turned out that for the limited space that is available no motor could be found that delivers more torque than the current Faulhaber 1717. However, there is another gearbox available that provides a higher transmission ratio than the current gearbox. The current gearbox is the Faulhaber 16/7 which has a transmission ratio 1:14 and a length of 38.1 mm. An alternative gearbox is the Faulhaber 15A, which can deliver a maximum transmission ratio of 1:152 and fit in the driving module. The Faulhaber 15A with a transmission ratio of 28:1 should be sufficient to provide the necessary torque. However, a higher transmission ratio decreases the driving speed. If this speed is of minor importance, this gearbox can be used.

4.3.3 Reducing Clamping Torque Friction

Instead of increasing the driving torque, which will reduce the driving speed, the friction caused by the clamping torque can be reduced. By reducing the deformation of the wheels, the friction can be reduced.

The deformation of the wheels can be reduced by using a smaller tire tread or other kind of rubber. The current wheels consist of natural rubber with a hardness of 50° shore, however natural rubber is available with a hardness up to 100° shore. Experimenting with different kinds of rubber and shape might create a more suitable trade-off between the traction and driving torque.

4.4.2 Driving Control

For autonomous driving, some control is also needed for the driving motors. To each driving motor, an incremental encoder is connected. This encoder is added to create a position or velocity feedback loop. However, only the motor current limit prevents stressing the motor during riding in the pipe. This limit cannot be configured to low, because of the high start up motor current. By only controlling the driving torque with the position or velocity feedback, no care can be taken to prevent the motors from excessive stressing. By controlling the torque with the motor current, both the torque and the current to the motor is controlled.

For driving autonomously, it is recommended to use position/speed control in combination with the motor current control.

4.5 Driving Module Conclusion

From the driving module analysis it can be concluded that the driving motors cannot provide the maximum necessary torque at the nominal motor current. This maximum necessary torque of approximately 131 mNm is necessary when the robot is driving sideways in the pipe under a slope of 30°, while the driving torque at the nominal motor current is approximately 120 mNm. All other manoeuvres should be possible to perform.

The efficiencies of the driving module are low. These low efficiencies are caused by friction between the gears. The driving speed is approximately 7 cm/s and less above driving torques of 120 mNm. This is less than the required manoeuvring speed of 8 cm/s. Because the bending speed is also low, the required manoeuvring speed cannot be supplied.

To increase the driving torque the current gearbox can be replaced by the Faulhaber 15A, which can deliver a maximum transmission ratio of 1:152 and fit in the driving module. The Faulhaber 15A with a transmission ratio of 28:1 should be sufficient to provide the necessary driving torque. However the driving speed will then decrease, because of these extra reductions.

Instead of increasing the driving torque, it would be better to reduce the friction caused by the clamping torque. Reducing the deformation of the wheels, by using a smaller tire tread or other kind of rubber will reduce these clamping friction. Experimenting with different kinds of rubber and shape might create a more suitable trade-off between the traction and driving torque.

For the driving module, the voltage loss in the local controller also has to be compensated when supplying voltage to the robot. For the driving module this voltage drop can get large because of the high motor currents.

For driving autonomously, it is recommended to use position/speed control in combination with the motor current control. This prevents stressing of the motor.

From the bending module analysis, it can be seen that there is a difference in clamping torques at the different motor currents (see chapter 3.3.2.2). As can be seen in table 4.1 and 4.2, there are no big differences in measured friction for the different motor currents. This is caused by the decreasing elasticity of the rubber at higher clamping torques. This means that the motor current can be used to control the clamping torque because the spread in measured friction torques is low.

5 Rotation Module

5.1 Introduction

In this chapter, the analysis of the rotation module will be discussed. In the prototype, there is one rotation module present as can be seen in figure 2.1. The function of the rotation module is to orientate the robot in a different direction. It rotates one half of the robot with respect to the other half. A schematic overview of the rotation module is shown in figure 5.1. The rotation module contains only one motor. The motor that is selected for the rotation module is the Faulhaber 1516 with a gearbox, which has a reduction of 1:809. This will theoretically provide an rotation torque of 380 mNm at the nominal motor current. To the motor, an incremental encoder and a homing sensor are added for control.

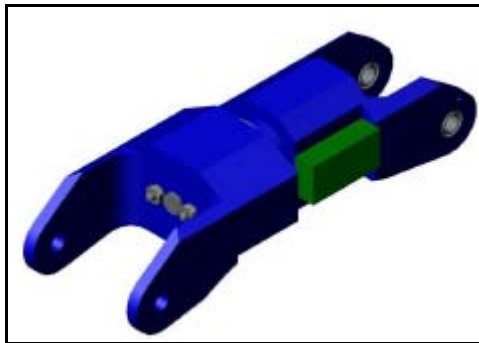


Figure 5.1: Schematic overview of the rotation module

5.2 Analysis of Current Rotation Module

The analysis of the rotation module starts with calculating the necessary rotation torque that has to be provided by the motors. During the detailing of the chosen pipe inspection robot concept, the calculation of the necessary rotation torque is carried out. (see [2]). From this calculation follows that a rotation torque of 300 mNm. should be sufficient for rotating the robot in the worst case scenario. This worst case scenario occurs if some wheels of the rotating half of the robot touches the wall in a pipe with a diameter of 119 mm.

In this calculation, estimates of the mass of half the robot (2 kg.) and friction coefficient (0.5) are used. However, from the analysis of the bending module the mass of the total robot is determined to be 1,5 kg. This reduces the necessary maximum rotation torque already to 220 mNm. This is calculated by using formula (17):

$$(17) \quad \tau_{rotation} = F_{friction} \cdot r$$

Here $F_{friction}$ is the friction force caused by the wheels that are touching the pipe wall, and r the arm of the momentum. Inserting the different parameters result in a necessary rotation torque of 220 mNm. This rotation torque is based upon a friction coefficient of 0.5.

This friction coefficient estimate is taken from the friction coefficient tests that are performed by J.J.G. Vennegoor op Nijhuis. For these tests, the friction coefficient is measured without taken any deformation of the wheel into account. Because during a rotation no extra pressure is applied on the rotating part by the bending module, this friction coefficient can be used.

5.3 *Rotation Module Conclusion*

From the theoretical analysis of the rotation module, it can be concluded that the rotation motor can deliver the necessary torque. During the analysis of the limitations of the current prototype, it has also been determined that the rotation module can practically deliver the necessary rotation torque in the worst case situation. Therefore, the rotation module does not have to be optimized.

6 Conclusions and Recommendations

6.1 Requirement Compliance

This report concludes with evaluating the performance of the total pipe inspection robot with respect to all the required manoeuvres which could not be met by the prototype. These manoeuvres are depicted in table 6.1.

Requirement	
Drive horizontally in straight pipe	✓
Rotate the robot	✓
Drive up a slope of 30°	✗
Drive through a bend (T-joint/Y-joint)	✗ ✓
Take a diameter change	✓
Average speed of 80 mm/s	✗

Table 6.1: manoeuvring requirements

The compliance to these requirements has been verified by using a pipe with a diameter of 119 mm, because here the highest necessary clamping torques are applied at the nominal motor current of 0.17 Ampere. The driving module motors are powered by supplying the power in direct PWM mode (without using control). The supplied voltage to the motors will be higher than the nominal motor voltage of 6 Volt, to compensate the voltage loss that occurs (see chapter 4.3.1). The maximum motor current for both driving modules is set to 0.7 Ampere, which is 0.2 ampere above the nominal motor current.

6.1.1 Manoeuvring Evaluation

The manoeuvres that are evaluated are:

- Driving sideways in a straight pipe. A driving torque of approximately 57 mNm (see chapter 4.2.1) per driving motor is necessary. Because the driving torque at the nominal motor current is 120 mNm (see chapter 4.3.1), which is more than sufficient.
- Driving horizontally in a straight pipe. A driving torque of approximately 84 mNm per driving motor is necessary (see chapter 4.2.1). Because the driving torque at the nominal motor current is 120 mNm (see chapter 4.3.1), which is more than sufficient.
- Driving sideways in a straight pipe under a slope of 30°. A driving torque of approximately 131 mNm per driving motor is necessary (see chapter 4.3.1), which is more than the driving torque at the nominal motor current (120 mNm at 0.5 Ampere). At a motor current of 0.7 Ampere, a maximum slope of approximately 15° can be taken. A reason for not meeting the necessary torque for driving sideways up a slope of 30° is that the wheels deform slightly when driving sideways, giving a reduction of the possible torque of 40 mNm.
- Driving horizontally up a slope of approximately 30°. Because no extra friction due to deformation of the wheels is present, the available driving torque is 130 mNm, which is sufficient to drive horizontally up a slope of 30°.

- Driving through a T-joint. The prototype can:
 - drive with one clamping module horizontally in the pipe
 - rotate itself in the pipe
 - drive sideways in the pipe

Note that the individual manoeuvres have been verified but the complete manoeuvre has not been verified because of time limitation.

- Average speed of 80 mm/s. As mentioned in chapter 3.5.1 and 4.3.1, the clamping speed (approximately 14 mm/s) and driving speed (approximately 70 mm/s) cannot satisfy the required average speed.

6.2 Recommendations

Mechanical recommendations:

- the motor housing material (bronze) of the bending module is not stiff enough. For fixing the bending motors and gears inside the motor housing, screws on the top of the motor housing need to be tightened. However, because the material is not stiff, the motor housing deforms slightly. This makes it difficult to place the motor and gears in a straight line. For this reason it is recommended to choose another material for the motor housing.
- To increase the driving torque, the current Faulhaber 16/7 gearbox with a transmission ratio of 14:1 can be replaced by the Faulhaber 15A gearbox with a transmission ratio of 28:1. This ratio should be sufficient to provide the necessary torque.
- Instead of increasing the driving torque, which will reduce the driving speed, the friction caused by the clamping torque can be reduced. By reducing the deformation of the wheels, the friction can be reduced.
The deformation of the wheels can be reduced by using a smaller tire tread or other kind of rubber. The current wheels consists of natural rubber with a hardness of 50° shore, however natural rubber is available with a hardness up to 100° shore. Experimenting with different kinds of rubber and shape might create a more suitable trade-off between the traction and driving torque. However, the friction coefficient between the wheel and pipe wall must not become too low. Therefore the friction coefficient has to be determined again after adjusting the wheels with the friction coefficient test setup (see 3.4.2)
- The gear train of the rear driving module is assembled with some eccentricity. Due to this assembly, the gear train is placed eccentric in the rear driving module. Due to this assembling, the gears of the driving module make bad contact with the gear that is attached to the wheel (see 4.4.1). Also the wheel rubber makes some slight contact with the gear housing of the rear module, which causes additional friction (see 4.4.1). This gear train needs to be reconstructed, to increase the efficiency of the rear driving module.
- The peg that fixates the gear trains of the driving modules need to be replaced by a screw. The peg can slide easily out the module, because it cannot stick enough to the gear train. (see 4.4.1)

- The gear that is directly connected to the actuated wheel at the front up bending module causes an extra low efficiency. The axis of this gear is constructed with some eccentricity and needs to be adjusted (see 3.5).

Electrical recommendations:

- The low pass filter at the output of the current sense interface of the local controller needs to be adjusted, in order to decrease the noise on the motor current measurement (see 3.3.2.2). This improves the accuracy of the PID controller.
- The low pass filter after the max1759 switching regulator of the local controller needs to be adjusted, in order to decrease the potentiometer ADC measurement noise. (see 3.3.1.3)

Control recommendation:

For driving autonomously, it is recommended to use motor current control, because this prevents excessive stressing of the motor. For the driving module, the motor current control needs to be combined with position/speed control. For the bending module the motor current control needs to be combined with the position control.

Appendix I Test case: Calibration of Clamp Torque Feedback

Introduction

An important part of the bending module are the torsion springs in the wheels which are located on both ends of the bending module. Figure AI.1 represents the assembly of these wheels.

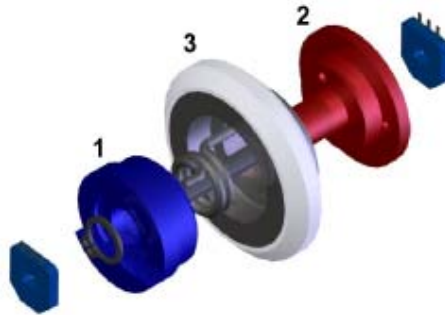


Figure AI.1: Assembly of wheels with torsion spring

This assembly consists of the wheel with a rim and two bodies with a torsion spring in between. The torque applied by the bending module is passed on to body number one and then again transferred to body two via the torsion spring. Body number two is connected to the adjacent module. If a torque builds up between two modules, the spring will elongate linear with the applied torque. By measuring the elongation, the build up torque can be determined.

The elongation is measured using a potentiometer that is connected to the shaft of body two and the housing of body one. The potentiometer is an analog sensor, and the signals that they generate are converted to ADC signals which are used as a feedback signal for the clamp torque. Calibration of this torque feedback is necessary to determine the amount of torque per ADC bit (Torque/ADC ratio).

Besides determining the ratio, the ADC value of the bending module when it is not bended (the spring is not elongated in this position), has to be determined. In the source code, this value will be used as a “zero point” for the clamp torque feedback.

Test Setup

As can be seen in figure AI.2, the bending module does slide sideways with the middle axis and the bottom wheels in a slit, which has the same length as the largest pipe diameter (119 mm). The friction that are caused by this sliding are kept minimal to have a good approximation of the clamp force.

For easy calculation, the bending is performed sideways to eliminate the gravitational force. To the bending module, a spring scale is attached to measure the applied clamp force. This spring scale has a range of 0 to 10 Newton. The following parts are also necessary for the test setup:

- Computer with software to control the bending module
- Two bending modules
- RS232 cable for communication
- Ruler (to measure the arm of momentum)

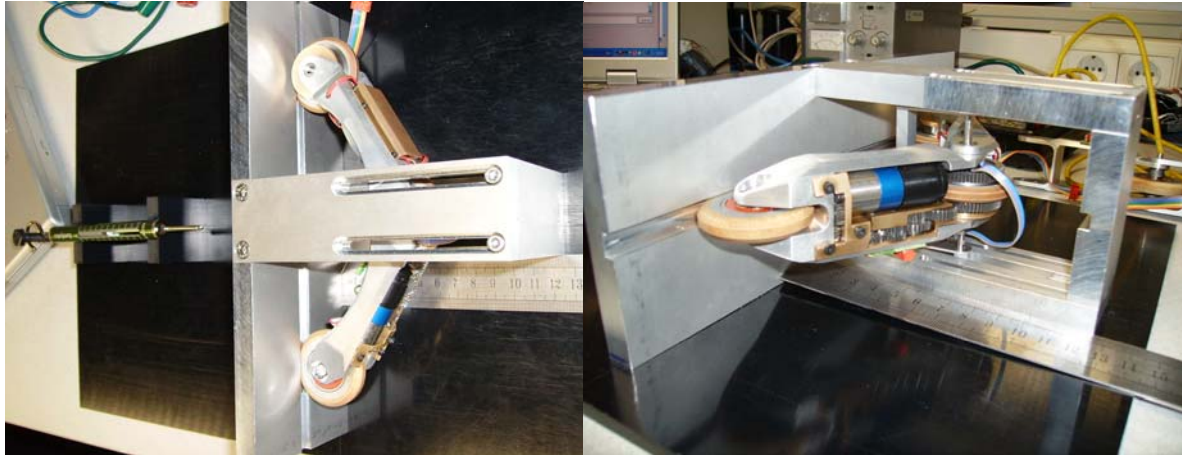


Figure AI.2: test setup for clamp torque calibration

Test case

The torque/ADC ratio will be measured by applying a force of 2 to 8 Newton with steps of 1 Newton. This limited clamp force is necessary to avoid stressing the torsion spring, which can handle a maximum clamp torque of 900 mNm.

The ADC value at the different applied clamping forces are read, and the length of the arm of the momentum is measured. This experiment is performed ten times to have a more accurate ADC value. The torque can then be determined with formula 1. Here the applied force is multiplied with the measured arm of the momentum (r):

$$(1) \quad \tau_{clamp} = F_{clamp} \cdot r$$

The torque/ADC ratio can then be determined with formula 2:

$$(2) \quad \tau / ADC \text{ ratio} = \frac{T_n - T_{n+1}}{ADC_n - ADC_{n+1}}$$

Here T_n and ADC_n are for example the torque and ADC measurements for a clamp force of 1 Newton and T_{n+1} and ADC_{n+1} the torque and ADC measurement for a clamp force of 2 Newton.

To be sure that after reassembling the bending module the torque/ADC ratio and setpoint remains the same, the entire experiment is repeated after reassembling the bending module. Here for, the bending module is first disassembled in two parts and the wheel in between is removed.

Besides the Torque/ADC ratio measurements, the ADC value of the bending module at a clamp force of 0 Newton will also be measured. This value will be the zero point of the clamping torque feedback.

Expected measurement results

Because the torsion spring has a linear characteristic, the Torque/ADC ratio is expected to be approximately constant for all applied clamp forces and is calculated as follows:

First the angle resolution is calculated with formula 3:

$$(3) \quad \theta_{resolution} = \frac{U_{ref} \cdot \theta_{max}}{U_{in} \cdot bit \text{ resolution}}$$

In this formula, U_{ref} is the reference voltage of the potentiometer (1.1 V), U_{in} is the input voltage of the potentiometer (3.3 V), θ_{max} is the maximum angle (333°) and the bit resolution is 1024. This gives an angle resolution of 0.1084°

The maximum torque that the torsion spring can handle is 900 mNm at a deflection of 24°. The maximum ADC output can be calculated with formula 4:

$$(4) \quad ADC_{max} = \frac{\theta_{max_spring}}{\theta_{resolution}} \approx 221$$

The torque/ADC ratio can be determined with formula 5:

$$(5) \quad \tau / ADC \text{ ratio} = \frac{T_{max_spring}}{ADC_{max}} = \frac{900}{221} \approx 4,1 \text{ mNm}$$

This means, that one ADC bit corresponds to a torque of 4,1 mNm. However, there is some backlash and friction present in both bending modules. This backlash and friction will probably influence the linearity of the torque/ADC ratio. From the measurement results, it have to be determined if this influence is problematic.

Measurement results

The mean measured ADC value at each applied clamp torque for the rear bending module is shown in figure AI.1. In this graph also the spread in the measurements is indicated. The dashed line with triangles indicates the maximum measured ADC value, and the dashed line with rectangles indicates the minimum measured ADC value.

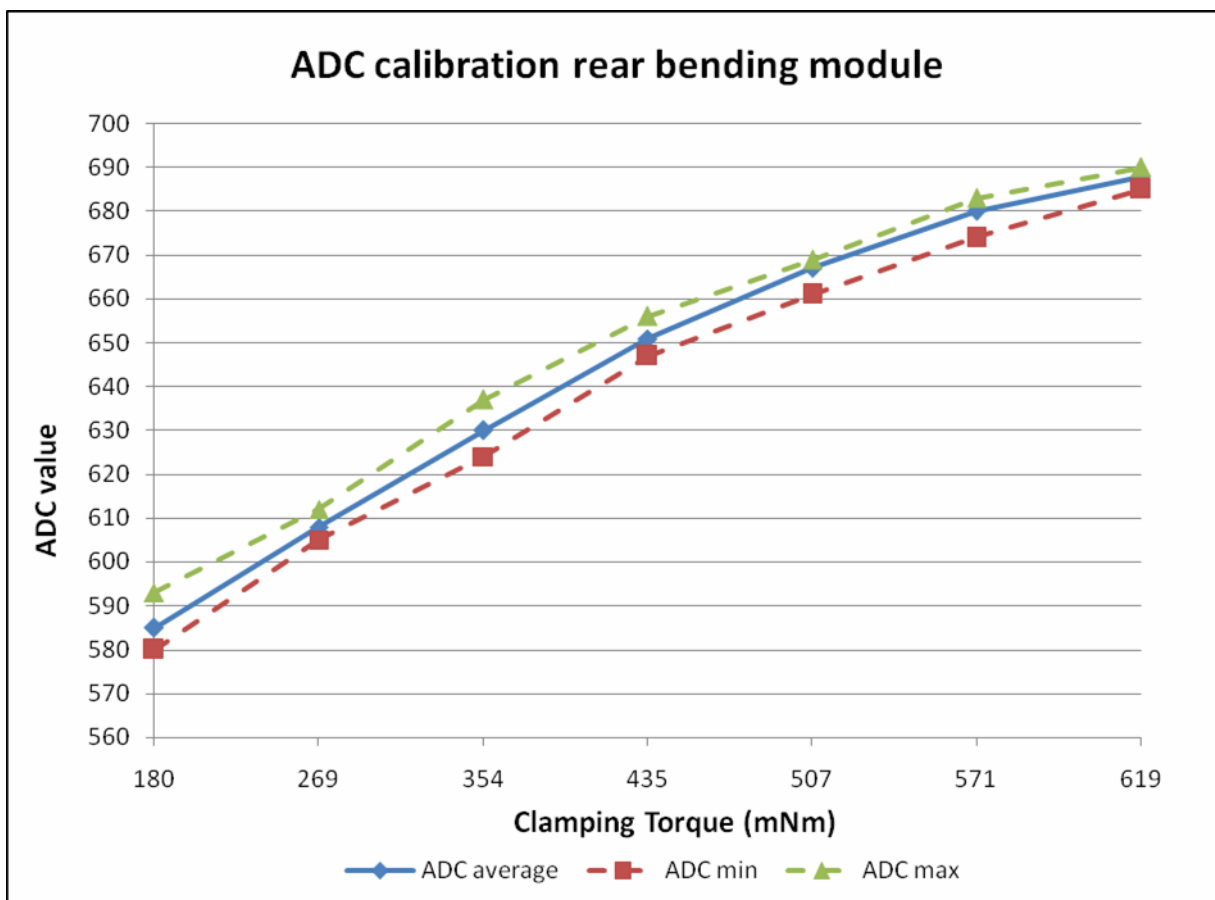


Figure AI.1: measured ADC values for the rear bending module

As can be seen, there is a non linear relationship between the applied clamp torque and the measured ADC value. It can also be observed that there is a spread in the measured maximum and minimum ADC values. This spread is caused by measurement noise and backlash and friction that are present in the bending module. To determine the measurement noise, tests are carried out on the ADC measurement. During these tests, the bending motors are fully powered and the potentiometer is kept at a fixed position. Figure AI.2 shows a graph of one of these tests where the difference in ADC measurements was the largest. This difference is 7 ADC bits, which explains a part of the measured ADC spread.

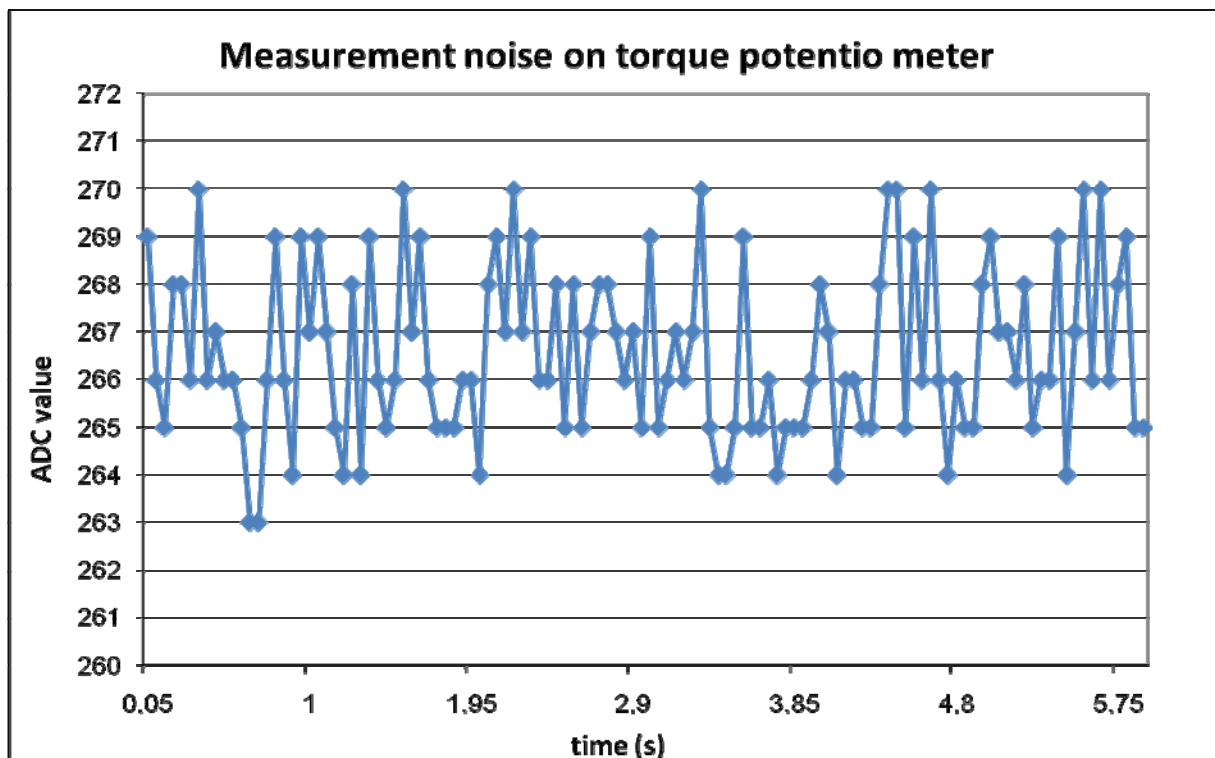


Figure AI.2: Measurement noise on torque potentiometer

This measurement noise is caused by the max1759 switching regulator, which converts the available battery voltage of 3.7V to a stable voltage of 3.3V. This 3.3V is the input voltage of the potentiometer. Figure AI.3 shows the schematics of this switching regulator.

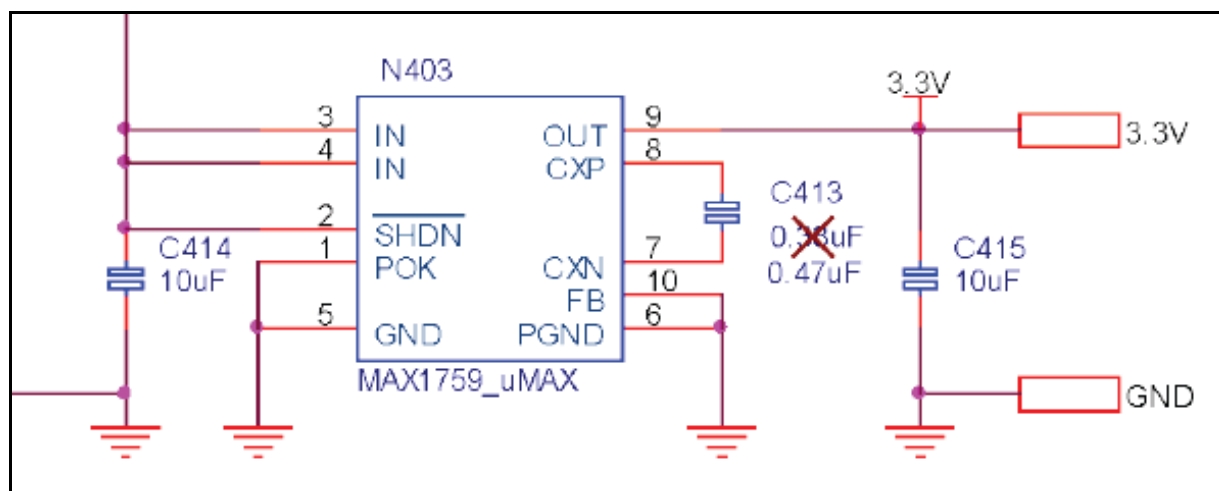


Figure AI.3: Schematic of the max1759 switching regulator

As can be seen in figure AI.3, there is a capacitor at the output of the switching regulator. This capacitor is used to produce a smooth output voltage. However, figure AI.4 shows that this output voltage is not stable and has the shape of a saw tooth.

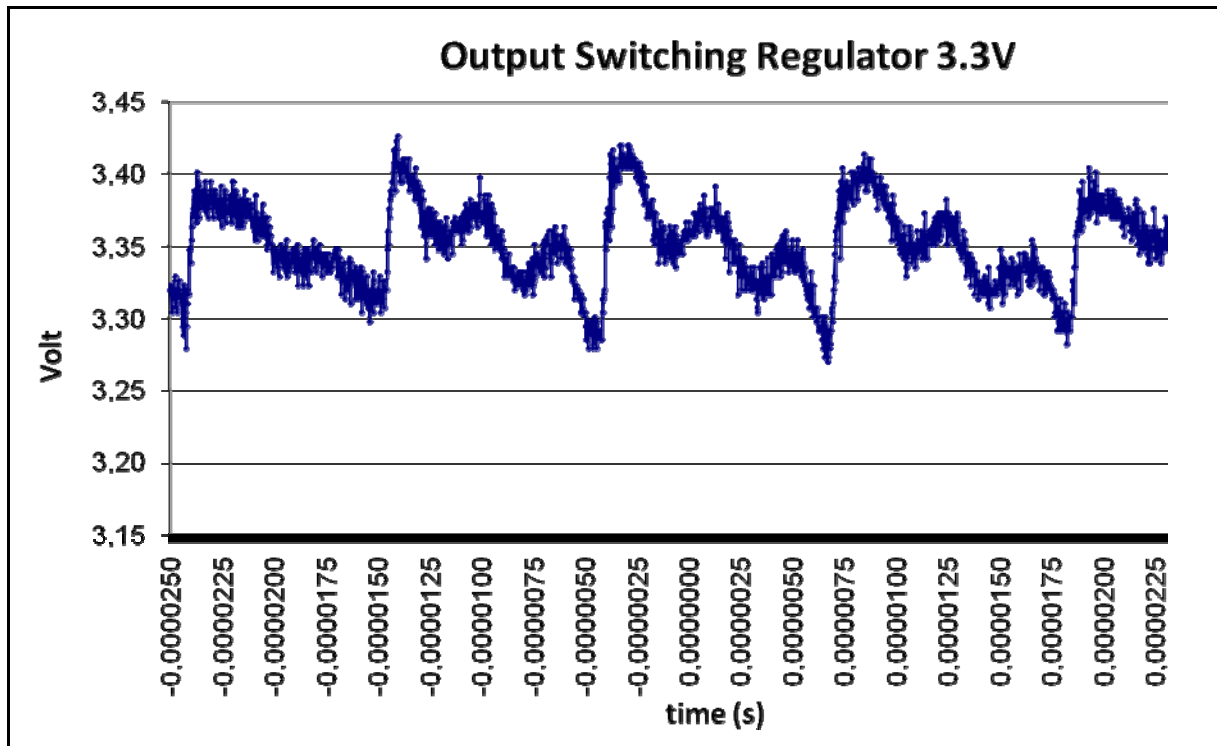


Figure AI.4: Output of the switching regulator

This output voltage of the switching regulator is also used as input voltage for the potentiometers. This causes the noise in the ADC measurements.

The other part of the measured spread in ADC values is probably caused by the friction and the backlash that is present in the bending module. It can be observed that the spread in measured ADC values is smaller for high clamping torques than for low applied clamping torques. This is probably caused by the backlash, which is less dominant at large applied clamping torques.

To be sure that, after reassembling the bending module, the torque/ADC ratio and setpoint remains the same, the entire experiment is repeated after reassembling the bending module. The measured ADC values at each applied clamp torque for the rear bending module after reassembling, are shown in figure AI.5.

As can be seen, also here a non linear relationship exists between the applied torque and the measured ADC value. For large applied clamp torques, it can also be observed that the spread in measured ADC values is smaller than for low applied clamp torques.

Besides these two observations, differ the measured ADC values after reassembling a lot. This is caused by reassembling the wheel. It is difficult to assemble the wheel exactly in the same position. For this reason it is not possible to determine a fixed setpoint for the clamp torque feedback.

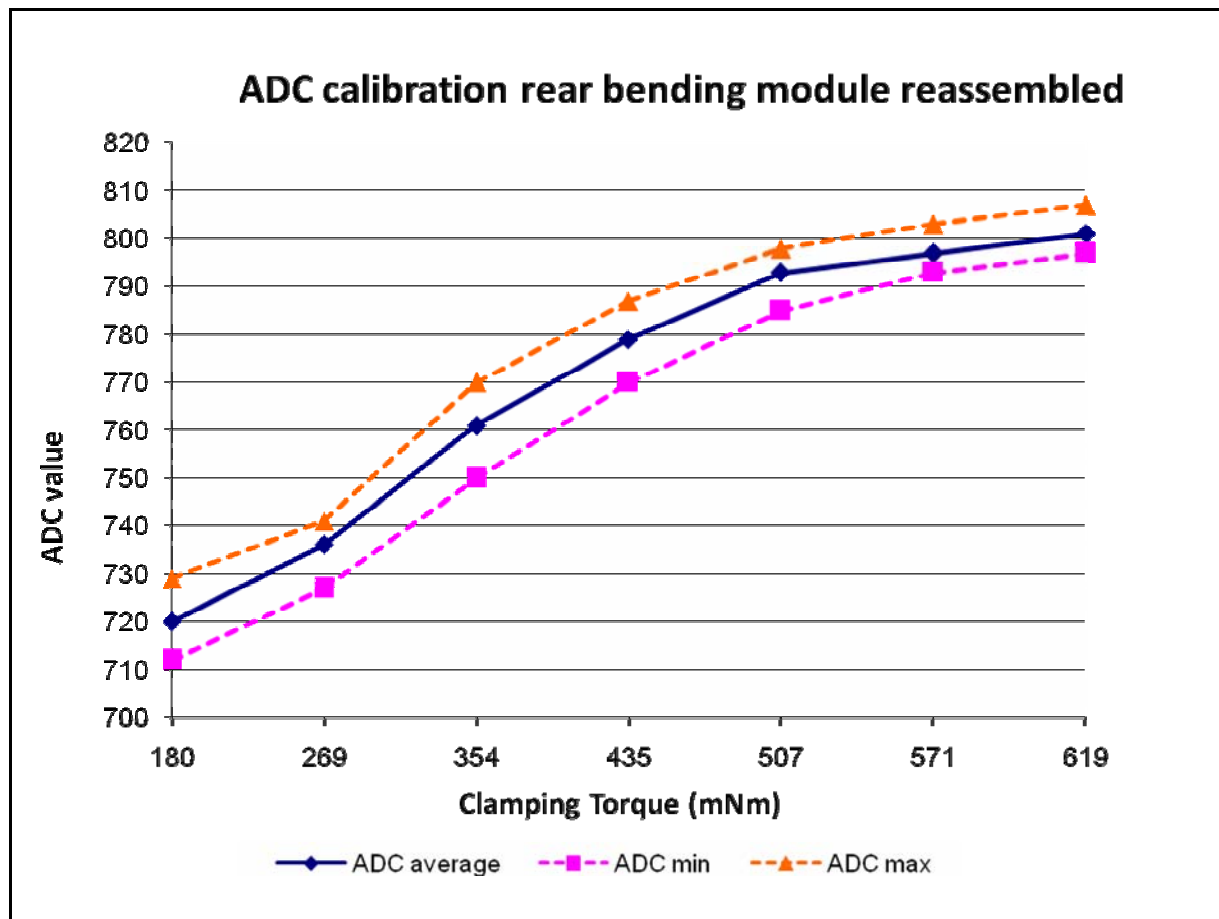


Figure AI.5: measured ADC values for the rear bending module after reassembling

The influence of the non linear relation (between the applied torque and the measured ADC values) on the Torque/ADC ratio can be seen in figure AI.6. In this graph, the Torque/ADC ratio for both measurements are shown. Only the average of the measured ratio's are used here. As can be seen, the straight line (first measurement) approximates the estimated constant torque/ADC ratio of 4,1 mNm/ADC for low clamp torques. At high clamp torques however, the ratio increases. The dashed line (representing the measurement after reassembling) shows very high ratio values for large clamp torques. This is caused by a small increase in the elongation of the torque spring, in comparison to the torque increase. For low clamp torques, the ratio is also not constant after reassembling.

To get a better overview of the spread in the measured ratio's at a certain clamp torque, the standard deviation and the mean of the measured ratio's, before and after reassembling, are presented in table AI.1.

Clamp Force (N)	First measurement		After reassembling	
	μ	σ	μ	σ
2 to 3	4.1	1.2	6.3	1.6
3 to 4	4.1	0.7	3.7	0.8
4 to 5	3.8	0.5	4.2	0.9
5 to 6	5.2	1.5	6.0	2.3
6 to 7	5.0	1.5	19.6	17.9
7 to 8	5.9	1.5	16.6	12.8

Table AI.1: standard deviation and mean of all measured ratio's for the rear bending module

In this table, σ is the standard deviation and μ the mean of all measured ratio's between two clamp forces. Optimal would be if the mean of the ratio's would be 4,1 and if the standard

deviation would be small. As can be seen does the mean ratio increase for increasing clamp forces. Also the standard deviation increases to a high value for the largest clamp forces.

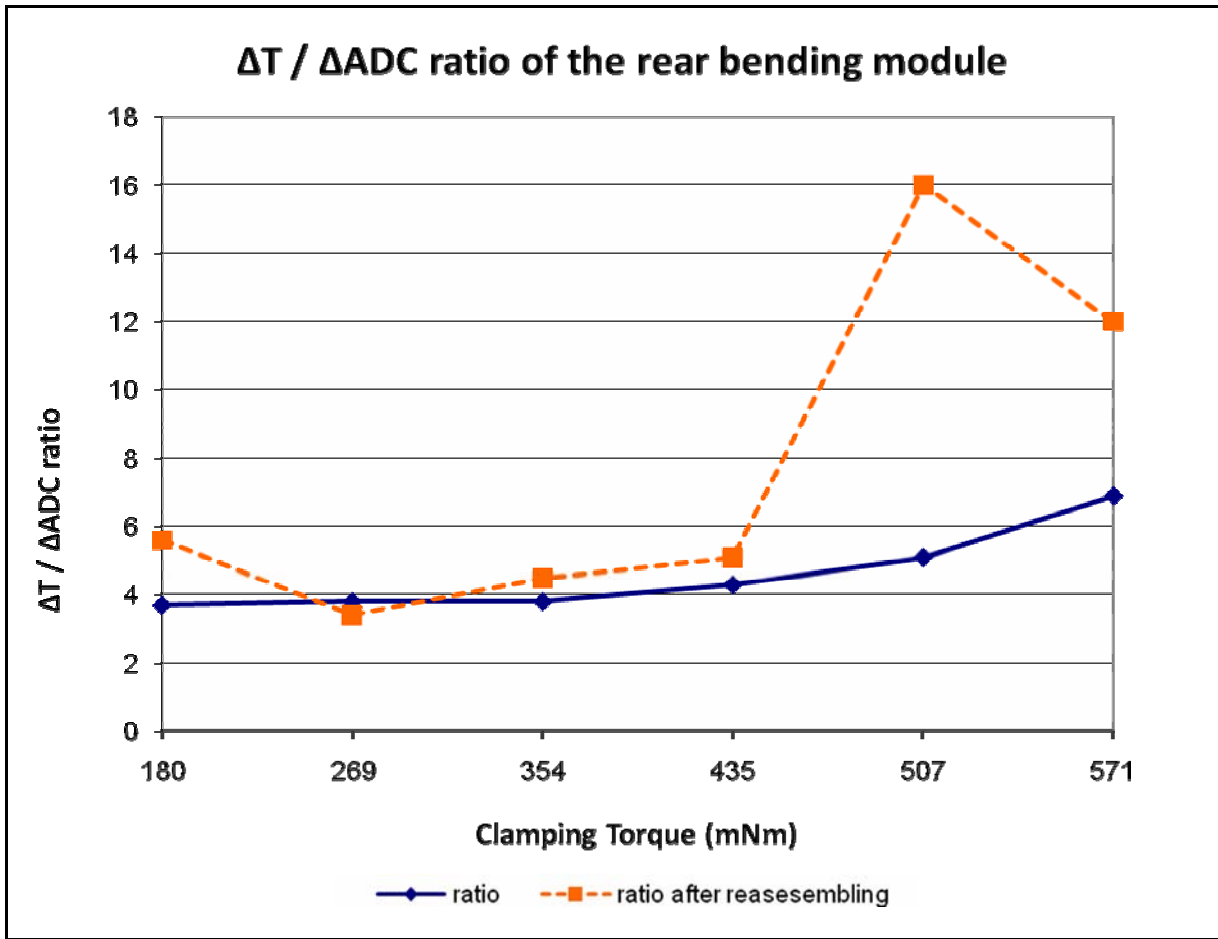


Figure AI.6: Calculated Torque/ADC ratio for both measurements (rear module)

The same test is carried out with the front bending module. The measured ADC values at each applied clamp force for bending the front bending module is shown in graph AI.7. In this graph also the spread in measurements is indicated. The same observations as for the front bending module can be applied to this graph. The difference between the rear bending module is that for a high clamp torques, the spread between the maximum and minimum measured ADC values is large.

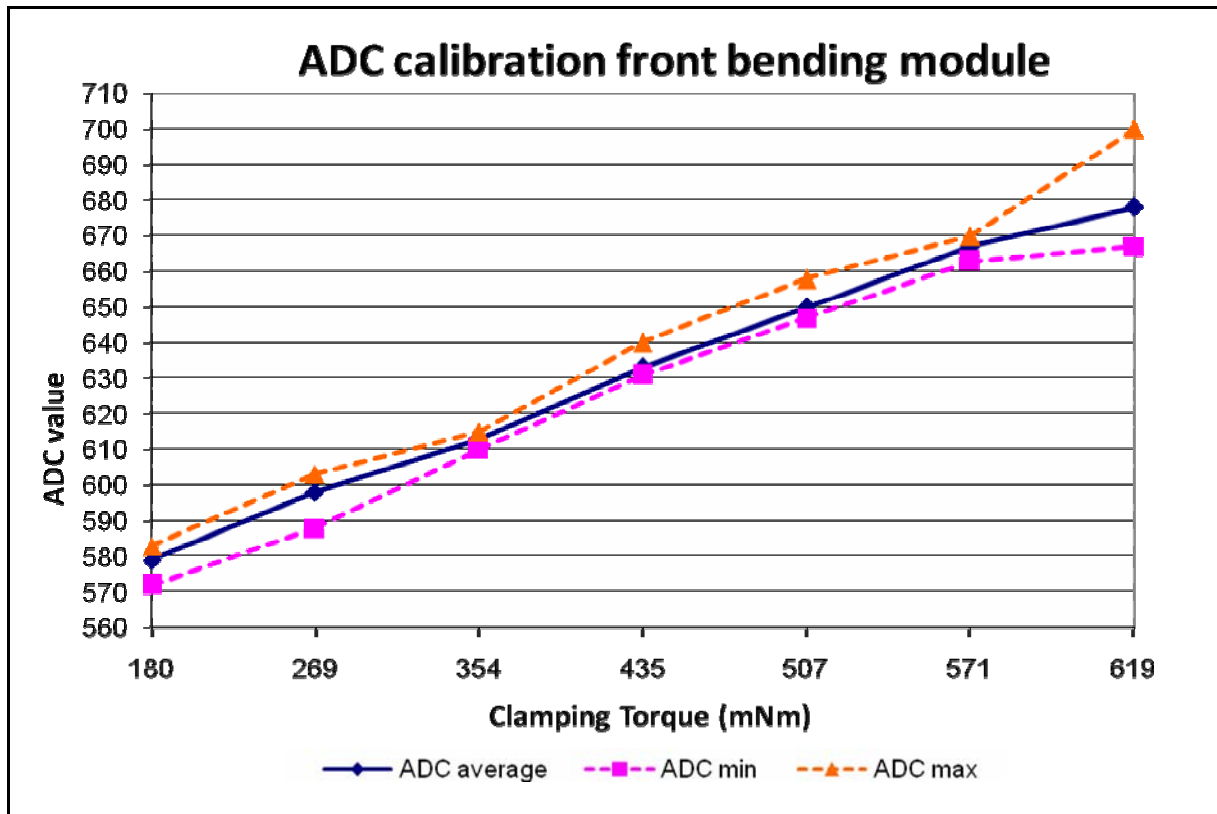


Figure AI.7: Measured ADC values for the front bending module

Also for the front bending module, the same test is carried out after reassembling. The test results are shown in figure AI.8. Also here, the measured ADC values after reassembling differ a lot. Here however, the spread in measured ADC values at high clamp torques reduce.

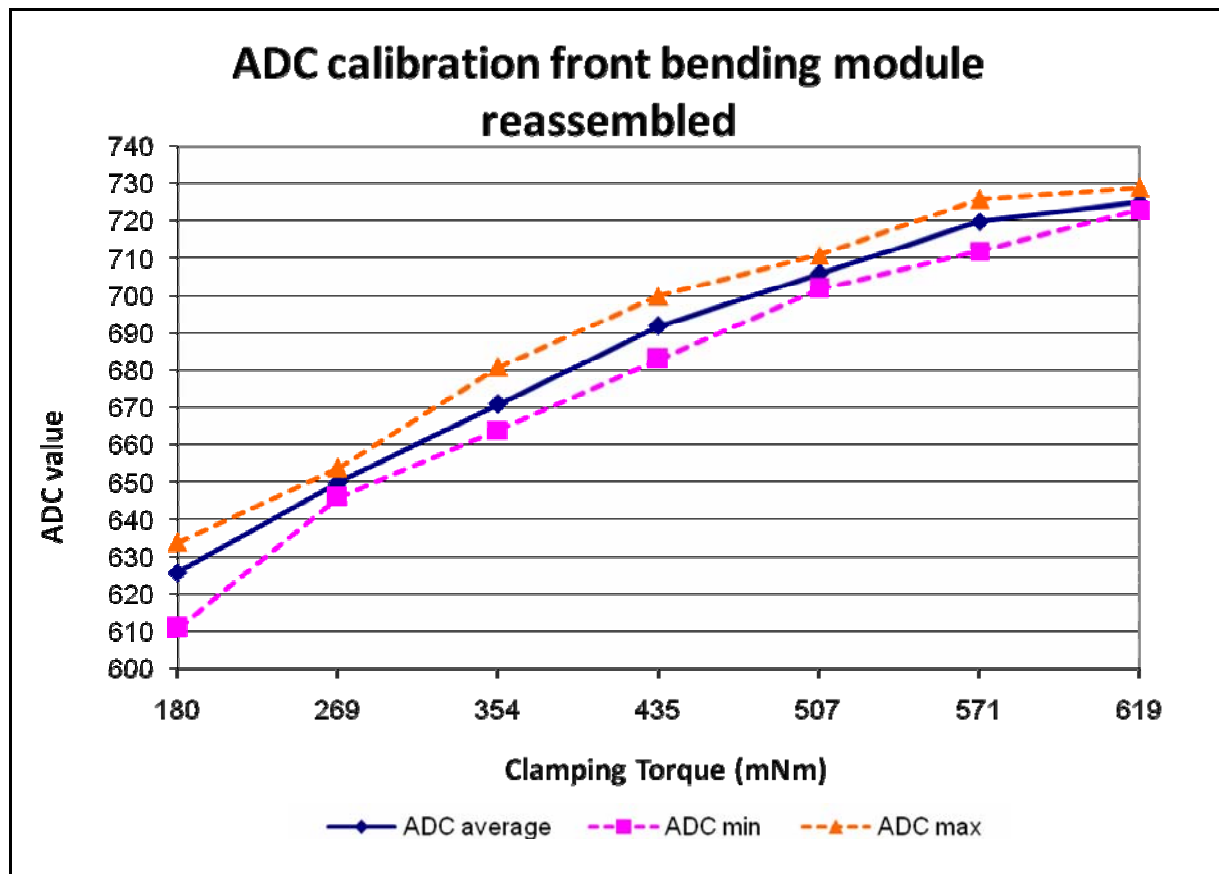


Figure AI.8: measured ADC values for the front bending module after reassembling

The influence of the non linear relation (between the applied torque and the measured ADC values) on the Torque/ADC ratio can be seen in figure AI.9. In this graph, the Torque/ADC ratio for both measurements are shown. Only the average of the measured ratio's are used here. Also for the front bending module it can be concluded that the Torque/ADC ratio is not constant.

To get a better overview of the spread in the measured ratio's at a certain clamp torque, the standard deviation and the mean of the measured ratio's, before and after reassembling the front bending module, are presented in table AI.2.

Clamp Force (N)	First measurement		After reassembling	
	μ	σ	μ	σ
2 to 3	4.9	1.5	3.8	0.6
3 to 4	6.3	1.8	4.4	1.2
4 to 5	4.1	0.5	4.0	1.6
5 to 6	4.2	0.3	6.9	4.4
6 to 7	4.1	0.9	4.4	1.3
7 to 8	6.6	3.4	19.4	16.1

Table AI.2: standard deviation and mean of all measured ratio's for the front bending module

As can be seen does the mean ratio increase for increasing clamp forces. Also the standard deviation increases to a high value for the largest clamp forces.

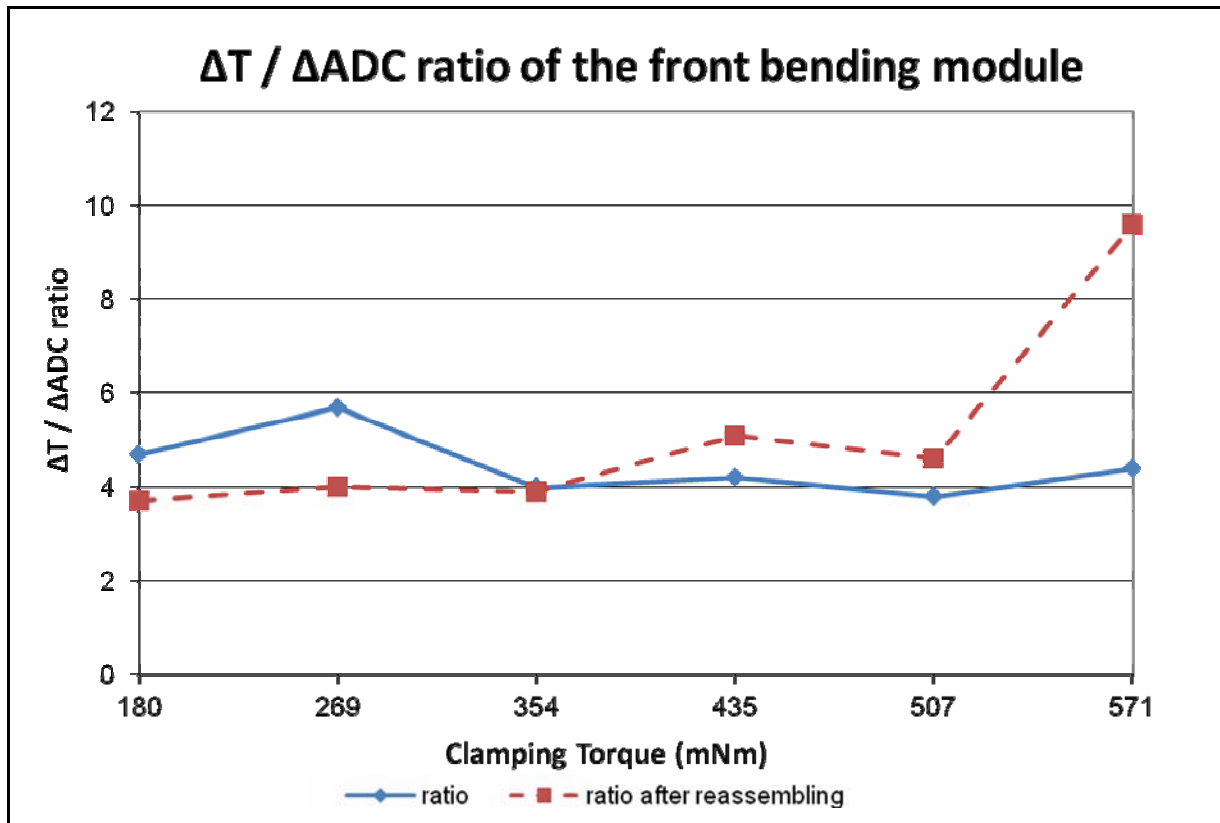


Figure A1.9: Calculated Torque/ADC ratio for both measurements (front module)

Appendix II Test case: Bending and Driving Efficiency

Introduction

With this test, the efficiency and the speed of the bending and driving module will be determined at certain motor loads. This information will be used for deciding if the motor and gears have to be adjusted in order to increase the clamp and driving speed of the robot.

Test setup

The test setup is shown in figure AII.1.

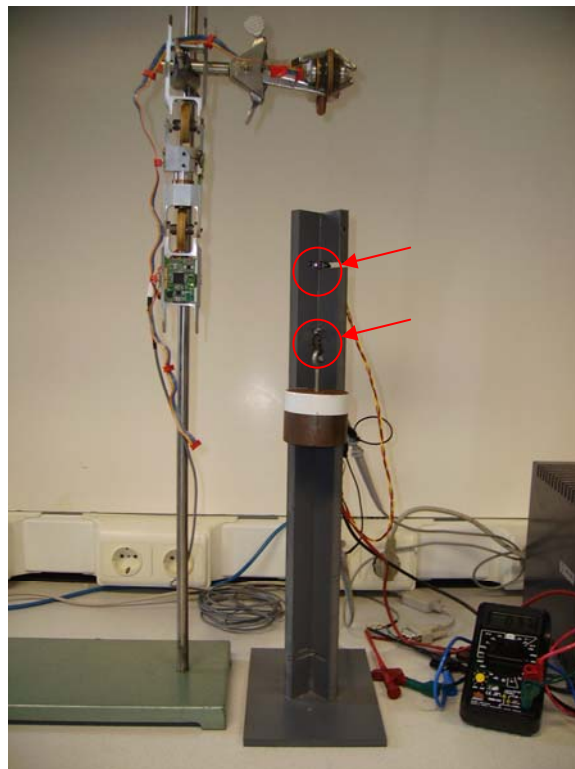


Figure AII.1: test setup

Dependent on the module which is tested, the test setup consist of the bending or driving module which is placed upon a stand. To the actuated wheel, a weight with a certain mass is connected with a wire. This weight slides through a gutter, which contains two photo micro sensors with a distance of 6.5 cm between each other. These sensors are indicated with the circles in figure AII.1. Other necessary parts are:

- A computer with software to control the bending module
- RS232 cable for communication
- Oscilloscope
- Stand
- 2 Multi meters (to read the motor current and the motor voltage)

Test cases

The efficiency of the bending module is determined by comparing the input power with the output power. The electrical input power can be calculated with formula 1:

$$(1) \quad P_{in} = U \cdot I$$

In this formula, U is the motor voltage in volts and I the motor current in amperes. The motor voltage and current can be measured with a multi meter.

The mechanical output power can be calculated with formula (2):

$$(2) \quad P_{out} = \tau \cdot \omega$$

Here, τ is the torque in Newton meters and ω the angular velocity in radians per second. The torque depends on the mass of the connected weight and can be calculated with formula 3:

$$(3) \quad \tau = m \cdot g \cdot r$$

Here, m is the mass of the weight in kilograms, g the gravitational acceleration (9.81) and r the arm of momentum in meters, which is the radius of the actuated wheel were the wire is connected to.

The angular velocity will be determined with the two photo micro sensors and an oscilloscope. If the weight passes a sensor, it will be detected by and the output voltage of the sensor will drop to zero. With the oscilloscope, the time between the voltage drops of both sensors can be determined. The angular velocity, in radians per second, can then be calculated by using formula (4):

$$(4) \quad \omega = \left(\frac{\left(\frac{d}{t} \right)}{2\pi r} \right) \cdot 2\pi$$

Here, d is the distance between the two sensors in centimetres and t is the travel time of the weight between the two sensors in seconds and R the circumference of the actuated wheel in metres.

The efficiency of the motor and gears can be calculated with formula 5:

$$(5) \quad Efficiency = \left(\frac{P_{out}}{P_{in}} \right) \cdot 100 \%$$

This test will be carried out for a few different applied torques, which can be varied with the mass of the weight. The test will also will be performed with direct supplying the power to the motors (nominal voltage) without using the local controller, and with supplying the power by using the local controller in direct PWM mode (without using control). It can then be decided if the local controller influences the efficiency of the motor and gears.

Measurement results of Bending module

The efficiency measurement results of the bending modules are presented here. Because both the rear and front bending module consists of two motors, four motors are evaluated. To make a distinction in these motors, they are indicated with up and down. The “up” motor is the one that is connected to the wheel which is actuated by the driving motor.

Rear bending module

The efficiency measurement results for the rear bending module “up” are presented in table All.1 and All.2.

Torque (mNm)	Motor voltage (V)	Applied Motor Current (A)	Speed (rad/s)	Power in (Watt)	Power out (Watt)	Efficiency
120	6.0	0.07	0.23	0.42	0.03	7%
150	6.0	0.08	0.22	0.48	0.03	7%
180	6.0	0.10	0.20	0.6	0.04	7%

Table AII.2: Efficiency rear up bending module without using local controller

Torque (mNm)	Motor voltage (V)	Applied Motor Current (A)	Speed (rad/s)	Power in (Watt)	Power out (Watt)	Efficiency
120	6	0.06	0.22	0.36	0.026	7%
150	6	0.07	0.20	0.42	0.03	7%
180	5.9	0.10	0.18	0.59	0.03	5%

Table AII.2: Efficiency rear up bending module with using local controller

The efficiency measurement results for the rear bending module “down” are presented in table All.3 and All.4.

Torque (mNm)	Motor voltage (V)	Applied Motor Current (A)	Speed (rad/s)	Power in (Watt)	Power out (Watt)	Efficiency
120	6	0.08	0.22	0.48	0.03	6%
150	6	0.10	0.19	0.60	0.29	5%
180	6	0.11	0.18	0.66	0.03	5%

Table AII.3: Efficiency front down bending module without using local controller

Torque (mNm)	Motor voltage (V)	Applied Motor Current (A)	Speed (rad/s)	Power in (Watt)	Power out (Watt)	Efficiency
120	6	0.07	0.20	0.42	0.024	6%
150	5.9	0.09	0.17	0.53	0.026	5%
180	5.9	0.10	0.17	0.59	0.03	5%

Table AII.4: Efficiency front down bending module with using local controller

Front bending module

The efficiency measurement results for the front bending module “up” are presented in table AII.5 and AII.6.

Torque (mNm)	Motor voltage (V)	Applied Motor Current (A)	Speed (rad/s)	Power in (Watt)	Power out (Watt)	Efficiency
120	6	0.08	0.22	0.48	0.026	6%
150	6	0.10	0.18	0.60	0.027	5%
180	6	0.12	0.17	0.72	0.03	4%

Table AII.5: Efficiency front up bending module without using local controller

Torque (mNm)	Motor voltage (V)	Applied Motor Current (A)	Speed (rad/s)	Power in (Watt)	Power out (Watt)	Efficiency
120	5.9	0.08	0.17	0.47	0.023	4%
150	5.9	0.11	0.15	0.65	0.025	3%
180	5.9	0.13	0.14	0.77	0.025	3%

Table AII.6: Efficiency front up bending module with using local controller

The efficiency measurement results for the front bending module “down” are presented in table AII.7 and AII.8.

Torque (mNm)	Motor voltage (V)	Applied Motor Current (A)	Speed (rad/s)	Power in (Watt)	Power out (Watt)	Efficiency
120	6.0	0.06	0.22	0.36	0.026	7%
150	6.0	0.08	0.21	0.48	0.030	7%
180	6.0	0.10	0.19	0.60	0.034	6%

Table AII.7: Efficiency front down bending module without using local controller

Torque (mNm)	Motor voltage (V)	Applied Motor Current (A)	Speed (rad/s)	Power in (Watt)	Power out (Watt)	Efficiency
120	5.9	0.06	0.22	0.35	0.026	7%
150	5.9	0.08	0.19	0.47	0.029	6%
180	5.9	0.09	0.18	0.53	0.032	6%

Table AII.8: Efficiency front down bending module with using local controller

As can be seen from these tables, the efficiencies of these motors and gears are approximately 5% to 7%. For the front up bending module, the efficiency decreases even to 3% to 6%. The extra low efficiency of this motor and gears is caused by the gear that is directly connected to the actuated wheel. The axis of this gear is deformed.

From the results we can see that for low angular velocities, the efficiency is lower than for high angular velocities. At low velocities the friction is larger, which causes the efficiency to decrease. The maximum measured speed of the bending motors is approximately 0.35 cm/s at a torque of 120 mNm. For larger torques this speed decreases to a measured minimum of 0.21 cm/s at a torque of 180 mNm. At higher torques, this bending speed will decrease even more.

It can also be seen that there is some motor voltage loss when the local controller is used. This is caused by the wire, which is connected between the power supply and the main control board of the robot, and the H-bridge. The wire has a resistance of approximately 1,5 Ω and the H-bridge has an internal resistance of 1.2 Ω . When the motor current increases,

the voltage drop in the wire and the H-bridge increases too. This means that the supplied (nominal) motor voltage has to be increased to compensate for these losses. However the dissipation in the wire is of minor importance in the future, because this wire is not used when the robot is moving autonomously.

Measurement results of Driving module

The efficiency measurement results of the bending modules are presented here. The robot consists of two driving modules, each containing one motor. Both the rear and front driving motors and gears motors are evaluated.

Front driving module

The efficiency measurement results for the front driving module are presented in table AII.9 and AII.10.

Torque (mNm)	Motor voltage (V)	Applied Motor Current (A)	Speed (rad/s)	Power in (Watt)	Power out (Watt)	Efficiency
66	6	0.29	6.2	1.74	0.41	24%
96	6	0.39	5.4	2.34	0.52	22%
120	6	0.50	5.4	3.00	0.65	22%

Table AII.9: Efficiency front driving module without using local controller

Torque (mNm)	Motor voltage (V)	Applied Motor Current (A)	Speed (rad/s)	Power in (Watt)	Power out (Watt)	Efficiency
66	5.3	0.29	5.4	1.54	0.36	23%
96	4.9	0.40	4.3	1.96	0.41	21%
120	-	-	-	-	-	-

Table AII.10: Efficiency front driving module with using local controller

Rear driving module

The efficiency measurement results for the rear driving module are presented in table AII.11 and AII.12.

Torque (mNm)	Motor voltage (V)	Applied Motor Current (A)	Speed (rad/s)	Power in (Watt)	Power out (Watt)	Efficiency
66	6	0.31	6.2	1.86	0.41	22%
96	6	0.44	5.4	2.64	0.52	20%
120	6	0.55	4.9	3.3	0.59	18%

Table AII.11: Efficiency rear driving module without using local controller

Torque (mNm)	Motor voltage (V)	Applied Motor Current (A)	Speed (rad/s)	Power in (Watt)	Power out (Watt)	Efficiency
66	5	0.31	4.8	1.55	0.32	21%
96	4.6	0.46	4.3	2.12	0.41	20%
120	-	-	-	-	-	-

Table AII.12: Efficiency rear driving module with using local controller

As can be seen from the efficiency measurement results of both driving modules, the efficiency of the motor and gears are approximately 18% to 24%. Also for the driving module the efficiency is higher at higher angular velocities. The maximum measured speed of the driving motors is approximately 9 cm/s at a torque of 66 mNm. For larger torques this speed decreases to a measured minimum of approximately 7 cm/s at the nominal motor current (0.50A).

It can also be noticed that the voltage losses when using the local controller are larger for the driving module than for the bending module. This is caused by the higher applied motor currents. At a torque of 120 mNm this voltage loss is decreased to such an extent that the weight cannot be lifted anymore and no efficiency can be measured. This voltage losses have to be taken into account when applying power to the motor.

Appendix III Test case: Calibration of Motor Current as Clamp Torque Feedback

Introduction

In order to decide if the motor current can be used to determine the clamp torque, tests have to be carried out. The “clamp torque/motor current” characteristic and the spread between measured torques at a certain motor current has to be determined.

Test setup

The test setup is shown in figure AIII.1. It consists of a balance and a construction where the “pipe wall” can be simulated with.

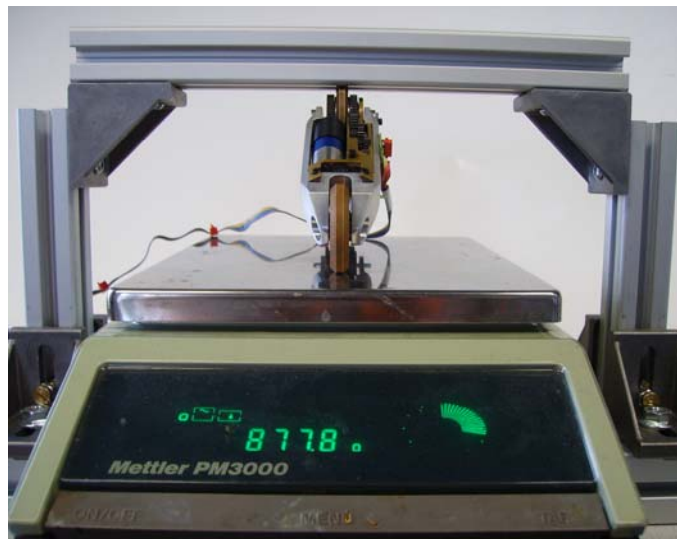


Figure AIII.1: test setup

The following parts are also necessary for the test setup:

- Computer with software to control the bending module
- Two bending modules
- RS232 cable for communication
- Multimeter to measure the motor current

Test case

During the test, the power supply delivers 6 volt to the robot. For a few motor currents from 0.12 Ampere up to the nominal current of 0.16 Ampere, which are controlled by using the motor current feedback, the clamp torque is calculated with formula 1:

$$(1) \quad \tau_{clamp} = m \cdot g \cdot r$$

In this formula, m is the mass that the balance indicates when the bending module clamps itself at a certain motor current between the balance and “pipe wall”, g is the gravitational acceleration and r the arm of momentum.

The “clamp torque/ motor current” characteristic have to be determined for the different pipe diameters, because this characteristic will probably differ for different pipe diameters (e.g. 57

mm and 119 mm.). For each motor current at a certain pipe diameter, the achieved clamp torque is measured ten times to determine the clamp torque spread.

Measurement results

Table AIII.1 shows the measured mean torques and the standard deviation at the applied motor currents and pipe diameters for the front bending module.

I (Ampere)	Diameter 57 mm.		Diameter 119 mm.	
	μ (mNm)	σ (mNm)	μ (mNm)	σ (mNm)
0.12	508	18	392	36
0.13	548	21	484	32
0.14	569	26	527	20
0.15	613	20	570	18
0.16	622	14	586	13
0.17	628	12	609	13

Table AIII.1: measured mean torque and standard deviation of front bending module

It can be seen that the clamp torque at a diameter of 57 mm is larger than for a diameter of 119 mm. We would expect that the clamp torque at a larger diameter would be equal to, or larger than the torque at a diameter of 57 mm. At a larger diameter the bending module has a larger normal force, which would compensate for the smaller arm of momentum. However the front bending module suffers from friction that is caused by the gear that is directly connected to the actuated wheel, as already mentioned in appendix II.

In order to decide if the motor current can be used for controlling the clamp torque, the spread in the measured torques at a certain current need to be small. As can be seen in table AIII.1, the spread in measured clamp torques is smaller for high clamp torques. The maximum spread is the highest at a diameter of 119 mm and for a motor current of 0.12. Here a standard deviation of 36 is measured, which means that 65% of the measured clamp torques differ 36 mNm from each other. In 95% of the measured clamp torques, this spread is 72 mNm, which is two times the standard deviation.

Table AIII.2 shows the measured mean torques and the standard deviation at the applied motor currents and diameter for the rear bending module.

I (Ampere)	Diameter 57 mm.		Diameter 119 mm.	
	μ (mNm)	σ (mNm)	μ (mNm)	σ (mNm)
0.12	548	13	550	26
0.13	554	12	579	16
0.14	575	9	640	18
0.15	601	10	663	17
0.16	618	12	681	15
0.17	654	12	684	14

Table AIII.2: measured mean torque and standard deviation of rear bending module

It can be seen that the clamp torque for the rear bending module at a diameter of 57 mm is smaller than for a diameter of 119 mm as expected. The measured clamp torques of the rear bending module are larger than for the front bending module. Also the standard deviation of the measured clamp torques is smaller than for the front module. This is in agreement to the efficiency test results of appendix II, where a lower efficiency is measured for the front module with respect to the rear module.

From table AIII.2, we can see that the spread in measured clamp torques is the highest at a diameter of 119 mm and for a motor current of 0.12. Here a standard deviation of 26 mNm is measured, which is smaller than the highest standard deviation of the front module.

Appendix IV Test case: Friction Coefficient

Introduction

In order to decide if the chosen bending motors can deliver the required torque, the friction coefficient has to be known. This friction coefficient is used for the theoretical calculations of the necessary clamping torque. In this section, the friction coefficient measurements are discussed.

Test setup

The test setup for measuring the static and dynamic friction coefficient is shown in figure AIV.1.

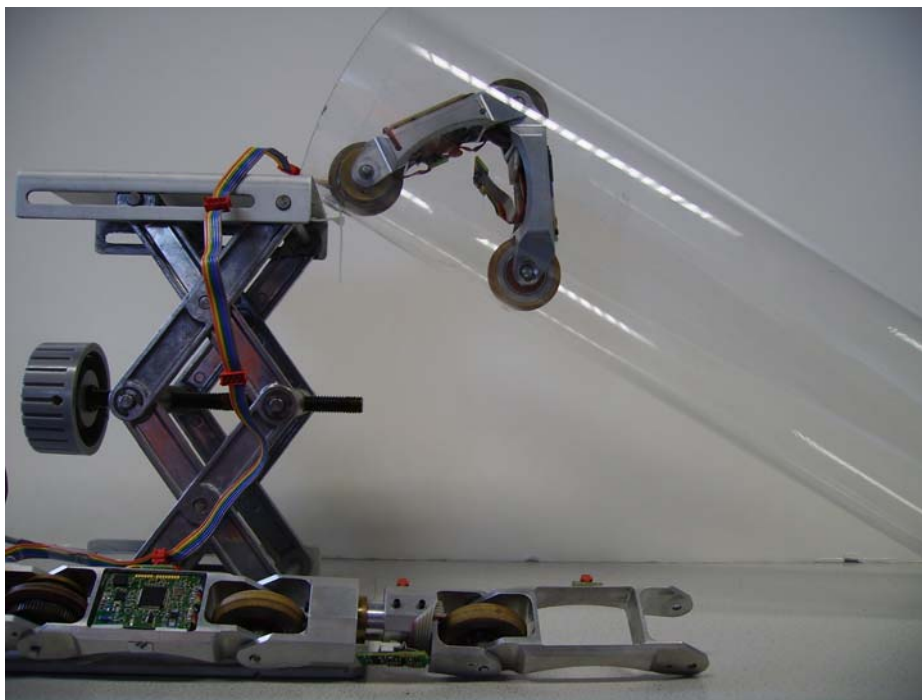


Figure AIV.1: test setup

The test setups consists of a bending module which is clamped inside the pipe. The wheels are fixed in this setup, such that they can only slide and not roll. The pipe is connected to a lift, which is used to set a certain angle between the pipe and the table. The following parts are necessary:

- Computer with software to control the bending module
- Two bending modules
- RS232 cable for communication
- One pipe with a diameter of 119 mm.
- Lift
- Ruler
- Video camera (only necessary for the dynamic friction coefficient)

Test cases

First the static friction coefficient is determined by using formula 1:

$$(1) \quad \mu_k = \frac{F_{friction}}{F_{normal}} = \frac{m \cdot g \cdot \sin \theta}{m \cdot g \cdot \cos \theta} = \tan \theta$$

In this formula is m the mass of the bending module, g the gravitational acceleration and θ the inclination angle at which the robot begins to slide. This sliding angle is determined by enlarging the inclination angle until the robot begins to slide. By using the height of the lift when sliding occurs and the length of the pipe, the sliding angle can be determined.

Because the friction coefficient is influenced by the applied clamp torque, the sliding angle is measured for a few different clamp torques. With these sliding angles, the static friction coefficient will be calculated.

After the static friction coefficient is determined, the dynamic friction coefficient is measured. To calculate the dynamic friction coefficient, the second law of Newton is used (formula 2):

$$(2) \quad F = m \cdot a$$

Where m is the mass of the part of bending module and a is the acceleration of the robot. From the calculation of the static friction coefficient we know that:

$$(3) \quad F_{friction} = \mu_k \cdot F_{normal} = \mu_k \cdot m \cdot g$$

When we combine the second law of Newton with this last equation (formula 3), it follows that the dynamic friction coefficient is equal to:

$$(4) \quad \mu_k = \frac{m \cdot a}{m \cdot g} = \frac{a}{g}$$

Because g is already known, the dynamic friction coefficient can be calculated when the sliding acceleration of the robot is determined. Because there is no encoder connected to the bending motors, the acceleration will be measured with a video camera and a ruler. The sliding motion of the bending module is recorded with the video camera, and then analysed with windows media player. With this application, the video can be slowed down to play one frame at a time. The sliding speed can then be measured by using formula 5:

$$(5) \quad V = \frac{d}{t}$$

Here, d is the distance the bending module travelled in centimetres and t is the number of frames the bending module travelled in this distance divided by 30. The acceleration can then be calculated with formula 6:

$$(6) \quad V^2 = V_0^2 + 2a \cdot \Delta x$$

In this formula is V^2 the squared measured speed, V_0^2 the squared initial speed, Δx the travelled distance and a the acceleration. Because the dynamic friction coefficient is also influenced by the applied clamp torque, the sliding acceleration is measured for a few different clamp torques.

For the static coefficient as well as for the dynamic coefficient test, the bending module is first clamped horizontal in an inclined pipe and secondly sideways. These two positions are used, because the wheels deform in both cases differently.

Measurement results

The measurements are performed in a pipe with a diameter of 119 mm. Here the rear bending module is clamped inside the pipe with a clamp torque of approximately 550 mNm. At this clamp torque, the friction coefficient cannot be measured because the robot does not slide even when the angle is 90°. This means that the friction coefficient is very high and far above the assumed friction coefficient of 0.3.

To measure the friction coefficient, the clamp torque has to be less than 550 mNm. Here for the motor current has to be far less than 0.12 Ampere. The bending motors are less efficient at these low motor current and clamp very slowly, which is not a good solution. Therefore it is pointless to measure the friction coefficient at these low motor currents.

Besides the static friction coefficient, also the dynamic friction coefficient cannot be determined because here for the robot has to be in motion.

Appendix V Test case: Maximum Necessary Driving Torque

Introduction

This test is carried out to get an approximation of the friction force caused by the clamping torque and rolling friction at different manoeuvres. Also the extra clamping torque caused by the reaction torque of the driving module itself, will experimentally be determined. These friction forces need to be overcome by the driving motors.

Test setup

The test setup is shown in figure AV.1.

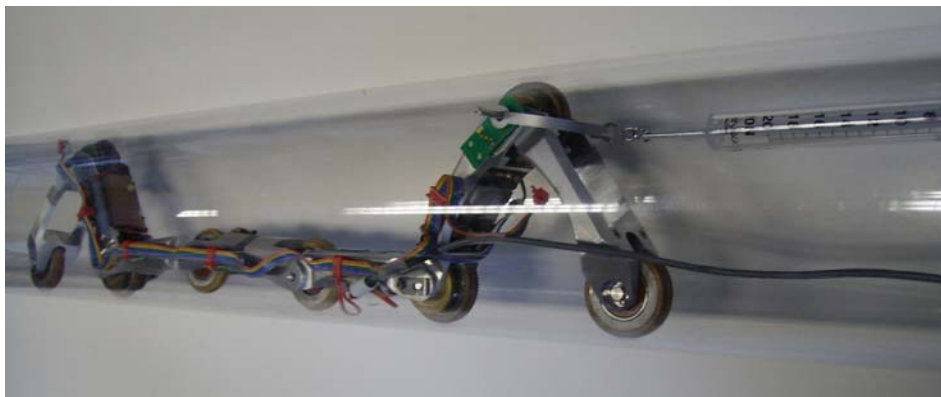


Figure AV.1: test setup

The test setups consists of:

- The total robot
- Computer with software to control the bending module
- RS232 cable for communication
- One pipe with a diameter of 119 mm
- Spring scale

Test case

First the friction caused by the clamping torque and rolling friction is determined for the different manoeuvres. These manoeuvres are:

- 5) One bending module clamps itself horizontal in the pipe (for the rear and front bending module)
- 6) Two bending modules clamp together horizontally in the pipe
- 7) Two bending modules clamping sideways in the pipe
- 8) Two bending modules clamping sideways in the pipe and driving up a slope of 30°

For all of these manoeuvres, a pipe with a diameter of 119 mm. is used, because here the highest clamping torques are achieved. Also the driving motors are removed, to rule out friction that are caused by the gears of the driving module.

The clamping is performed for motor currents from 0.12 Ampere to 0.17 Ampere. The friction is measured with a spring scale, which is attached to the bending module. This can be seen in figure AV.1. The force where the wheels begin to turn, is the friction force. These friction forces are determined 5 times to have a more accurate approximation.

Secondly, the extra clamping torque caused by the reaction torque of the driving module itself, will experimentally be determined. This is done by clamping one bending module inside the pipe with the driving motor reattached. The spring scale will also be attached to the bending module. Then the driving force is measured with the spring scale, when the robot is moving forward and when it is moving backwards. The half of the difference between these two driving forces is approximately the extra friction caused by the driving direction.

The maximum necessary driving torque is then calculated with formula 1:

$$(1) \quad \tau_{drive} = F_{max} \cdot r$$

In this formula is F_{max} the maximum friction force that the driving modules have to overcome and r the arm of the momentum. This arm is equal to the radius of the wheel, which is 0.02 meter.

Besides the already mentioned manoeuvres, the manoeuvre where the two bending modules clamp sideways in the pipe under a slope of 30° is determined theoretically. This is determined theoretically because it is difficult to measure with the proposed test setup.

Measurement results

The measured friction caused by the clamping torque and the rolling friction are presented in table AV.1 to AV.4. In this tables, the measured mean friction force and the standard deviation are given.

I (A)	0.12	0.13	0.14	0.15	0.16	0.17
Mean (N)	2.8	3	3.1	3.1	3.2	3.2
σ (N)	0.16	0.21	0.07	0.1	0.04	0.05

Table AV.1: Friction measured for maneuver 1 with front bending module

I (A)	0.12	0.13	0.14	0.15	0.16	0.17
Mean (N)	3	3.1	3.1	3.2	3.2	3.3
σ (N)	0.07	0.06	0.06	0.06	0.07	0.04

Table AV.2: Friction measured for maneuver 1 with rear bending module

I (A)	0.13	0.15	0.17
Mean (N)	4.1	4.2	4.3
σ (N)	0.13	0.05	0.11

Table AV.3: Friction measured for maneuver 2

I (A)	0.13	0.15	0.17
Mean (N)	4.5	4.6	4.7
σ (N)	0.12	0.19	0.07

Table AV.4: Friction measured for maneuver 3

From appendix III, we know that there is a large difference in clamping torques at the different motor currents. However, as can be seen in table AV.1 and AV.2, there are no big differences in measured friction for the different motor currents. The friction depends for a large part on the deformation of the wheel rubber. To increase the deformation of this rubber, the clamp torque has to increase. At a large deformation, the elasticity of the rubber will decrease and relatively more clamp torque has to be applied to deform the rubber. This explains the small difference in friction forces and the small increase in friction force at higher clamp torques. The maximum measured standard deviation is 0.21 Newton, which means that the spread in measured friction forces is small. The maximum measured difference in friction force is 0.5 Newton.

Because the friction force differs not much between applied motor currents, the friction force for manoeuvre 2 and 3 are only measured for 3 motor currents. These friction forces have to be overcome by both driving modules. This means that the friction for manoeuvre 2 and 3 per driving module is less high than for manoeuvre 1. We can also observe a difference between the friction force when driving horizontally in the pipe and driving sideways in the pipe. This is caused by the different deformation of the rubber wheels. The maximum measured standard deviation is for these two manoeuvres 0.19 Newton. Also here the maximum measured difference in friction force is 0.5 Newton.

Also the extra clamping torque caused by the reaction torque of the driving module itself, is experimentally determined. Table AI.5 presents the measurement results.

I (A)	0.7	0.8	0.9
Torque(N)	0.3	0.35	0.4

Table AV.5: Extra clamping torque caused by the reaction torque

As can be seen is the extra clamping torque approximately 0.3 Newton at a motor current of 0.7 Ampere. This needs to be added or subtracted (depends on the driving direction) to the friction forces determined in the measurements where just one module actuates the robot. When two driving modules are used, this extra friction force is added to the front and subtracted from the rear driving module, or vice versa. This approximately cancels the extra friction.

For manoeuvre 4, the necessary driving torque is the highest per driving module. This is because some extra torque needs to be applied to “push” the robot up the slope. This extra torque can be calculated with formula 2:

$$(2) \quad \tau_{push} = m \cdot g \cdot \sin(\alpha) \cdot r$$

In this formula is m the mass of the robot (1.5 kg.), g the gravitational acceleration (9.8 m/s), α the slope (30°) and r the arm of momentum (0.02 m). The total ‘push’ torque at 30° is almost 147 mNm. Per motor, an extra torque of approximately 74 mNm has to be delivered.

References

- [1] Edwin Dertien. System Specifications for PIRATE. Edwin Dertien, Control laboratory, University of Twente, the Netherlands, 2006
- [2] Jeroen Vennegoor op Nijhuis. Development of a pipe inspection robot. University of Twente, 2007
- [3] Jos Ansink. Electronic design for a gas pipe inspection robot. Control Laboratory, University of Twente, the Netherlands, 2007.
- [4] ATMEL. *AVR221: Discrete PID controller*. <http://www.atmel.com>, 2006
- [5] MPC17531A H-bridge datasheet.
http://www.freescale.com/files/analog/doc/data_sheet/MPC17531A.pdf, 2008
- [6] MAX1759 current sense amplifier datasheet.
<http://datasheets.maxim-ic.com/en/ds/MAX1759.pdf>, 2008